Intermediate stages of the Rydberg-level population of multiply charged ions escaping solid surfaces

N. N. Nedeljković[*] and M. D. Majkić
Faculty of Physics, University of Belgrade, P. O. Box 368, Belgrade, Serbia
(Received 8 June 2007; published 9 October 2007)

We have investigated the intermediate stages of electron capture into Rydberg states of multiply charged ions (core charge $Z \gg 1$, principal quantum number $n_A \gg 1$) escaping solid surfaces at low velocity. The time-symmetrized, two-state vector model of the process is proposed by using both initial and final states of the ion-surface system. The two conditions determine two wave functions and both are used to describe the system at intermediate stages. The appropriate probabilities and rates are defined and calculated from the corresponding mixed flux. Taking into account both the surface polarization and the polarization of the electronic cloud of the ionic core, the probabilities and rates are obtained in a simple analytical form; the population of the Rydberg levels of the ions Ar VIII, Kr VIII, and Xe VIII interacting with an Al surface is considered as an example. The quasiresonant character of the process is demonstrated, as well as the complementarity of the neutralization and ionization processes for the A^{Z+} ions escaping the surface and the $A^{(Z-1)+}$ ions approaching the surface, respectively. The neutralization distances for the ions finally detected in a given Rydberg state are obtained from the calculated rates. Although defined under different physical conditions, the results obtained are in agreement with the coupled-angular-mode theoretical predictions.

I. INTRODUCTION

Electron exchange during the interaction of ions with solid surfaces has been studied intensively both theoretically and experimentally; namely, understanding of the ionization and neutralization processes is essential for describing a variety of complex surface processes (plasma-wall interaction, plasma processing of materials, nanoscale electronic devices, arrangement of the ions on the surface, surface chemical reactions, surface analytic methods, etc.). Aside from the practical relevance, the investigation of the intermediate stages of electron transfer offers the possibility of testing some new theoretical concepts; for example, the problem can be formulated in a time-symmetric way.

Up to now, several theoretical models and approaches for an investigation of the electron exchange processes have been proposed; here we mention the classical over-barrier (COB) method [1,2], and its extended dynamic version [3,4], the perturbation method [5], the coupled-angular-mode (CAM) method [6,7], the complex scaling method [8–11], the stabilization method [12,13], and the time-dependent close-coupling technique [14,15]. We also mention the recently formulated wave packet propagation approach [16]. The following two methods (in some cases combined) have also been proposed: the etalon equation method (EEM) [17–19] suitable for description of resonant ionization, and the two-state vector model (TVM) [20–23], for the time-symmetrized description of the neutralization processes.

Treatments of the electron exchange between a highly charged ion (core charge $Z \gg 1$) and a conducting solid surface can be classified according to the direction of the ionic motion (approaching or escaping the surface) and according to the range of the ionic velocities v. The basic process characteristic of ions slowly approaching the surface ($v \ll 1$ a.u.) is stepwise resonant neutralization, in which the electrons are successively captured into Rydberg states ($n_A \gg 1$); for a review, see Ref. [1]. Recently [19], the problem of ionization of these ions was treated independently of the neutralization problem. It was found that, for any given $Z \gg 1$, there are such Rydberg states, with sufficiently high n_A values, where the resonant ionization ends before the neutralization cascade has begun.

Theoretical studies [21–23] of one-electron capture into Rydberg states of multiply charged ions (neutralization) escaping the surface have been performed in the intermediate velocity range ($v \approx 1$). It was demonstrated that the intermediate stages of the ion-surface interaction require more details in quantum dynamics; thus the appropriate TVM was developed. Also, it was demonstrated that a back transfer of active electrons from the moving ion into the solid, i.e., the reionization of previously populated states, can be important for some Rydberg states [17]. The theoretical studies mentioned were focused on the final population probabilities P^{fin}; they were sufficient to explain the available results of beam-foil experiments.

In the present paper, we analyze electron capture (neutralization) into Rydberg states of multiply charged Rydberg ions escaping solid surfaces at low velocity, considering the ion-surface system within the time interval between initial and final "measurements." We adapt the TVM to the low-velocity case and the intermediate stages of the process; namely, instead of calculating the final probabilities P^{fin}, we consider the intermediate probabilities and rates. The main output of this analysis, from the standpoint of an experiment, is the neutralization distances R_c^N for the ions finally detected in a given Rydberg state. We point out that, up to now, direct observation of the electron exchange "localization" was experimentally performed only for the ionization of neutral Rydberg atoms ($Z=1$) [24,25] and H_2 molecules [26] slowly

*hekata@ff.bg.ac.yu

approaching solid surfaces. The localization of the electron capture into a particular (critical) Rydberg state of multiply charged ions under grazing impact can be deduced from the measured projectile kinetic energy gains [27,28]. The first neutralization distances so estimated for the stepwise neutralization correlate with the corresponding R_c^N values obtained in the present paper.

The TVM of the intermediate stages of the Rydberg level population represents a form of the time-symmetric formulation of quantum mechanics introduced by Aharonov *et al.* [29], and formulated in a closed mathematical form in Ref. [30]. Independent of the cited references, the Demkov-Ostrovskii type of two-state vector model [31] has been introduced in surface physics in Ref. [20], in which proton neutralization was considered; the model was further elaborated in Refs. [21–23] devoted to the neutralization of highly charged ions. Within the framework of the TVM, the state of a single electron is described by two state vectors $|\Psi_1(t)\rangle$ and $|\Psi_2(t)\rangle$. The first state evolves (in the first scenario) from the initial state $|\Psi_1(t_{in})\rangle = |\mu_M\rangle$ toward the future. The second state evolves "teleologically" (in the second scenario) toward the fixed final state $|\Psi_2(t_{fin})\rangle = |\nu_A\rangle$ detected at the final time $t = t_{fin}$. The states $|\Psi_1(t)\rangle$ and $|\Psi_2(t)\rangle$ are characterized by the parabolic quantum numbers μ_M of the electron initially localized in the solid and the spherical quantum numbers ν_A of the electron finally detected in the ion, respectively.

In the proposed model, the result of any measurement performed in the time $t \in (t_{in}, t_{fin})$ depends on both the initial and final quantum conditions (μ_M and ν_A). The TVM enables us to define [20–23] the two-state probability amplitude $A_{\mu_M,\nu_A}(t)$ and the corresponding probability $T_{\mu_M,\nu_A}(t)$. In the Rydberg-level population problem discussed in the present paper, we define the neutralization probability $P_{\nu_A}(t)$ as a "sum" over the initial quantum numbers μ_M of the quantity $T_{\mu_M,\nu_A}(t)$; for description of the intermediate stages of the process we use the normalized probability $\tilde{P}_{\nu_A}(t) = P_{\nu_A}/P_{\nu_A}^{fin}$, and the corresponding rate $\tilde{\Gamma}_{\nu_A}(t)$.

By definition, the quantity $\tilde{P}_{\nu_A}(t)$ represents the neutralization probability at time t under the condition that the state $|\nu_A\rangle$ is populated at time $t \to t_{fin}$. In the treatment of intermediate stages of neutralization, the polarization of the solid as well as the polarization of the electronic cloud of the ionic core is taken into account. The basic physical quantity in the calculation of $\tilde{P}_{\nu_A}(t)$ [20–23] is the mixed flux through the moving Firsov plane S_F, separating the solid and the ionic subsystems. We point out that the mixed flux, outside the time-symmetrized context, was introduced by Bardeen [32]. The wave functions $\Psi_1(\vec{r}, t)$ and $\Psi_2(\vec{r}, t)$ that constitute the mixed flux will be considered within the framework of the quasistationary approximation and calculated with asymptotic accuracy. Our attention will be focused on ionic states with large eccentricities (low-l_A states).

This paper is organized as follows. In Sec. II the general formalism of the TVM is presented. In Sec. III we derive expressions for the mixed flux and the intermediate probabilities and rates. In Sec. IV we present explicit results considering the Rydberg-level population for ions Ar VIII, Kr VIII, and Xe VIII (all with core charge $Z = 8$); the probabilities and
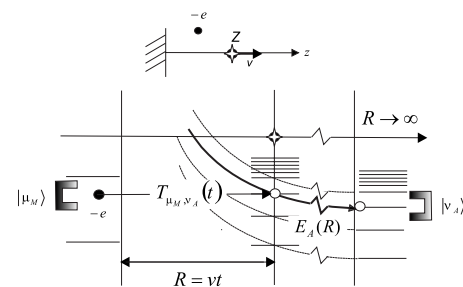

FIG. 1. Schematic time-symmetrized description of neutralization.

rates obtained will be compared with the CAM [7] results. The calculated neutralization distances R_c^N for the cited ions will be compared with the EEM [19] ionization distances; for the particular critical quantum number, the neutralization distances will be compared with the values estimated by the COB model, as well as with the values deduced from the available energy gain experimental data [27,28]. The concluding remarks are given in Sec. V.

Atomic units ($e^2 = \hbar = m_e = 1$) will be used throughout the paper unless indicated otherwise.

II. FORMULATION OF THE PROBLEM

A. Neutralization in two scenarios

We consider electron capture into the Rydberg state of multiply charged ions (core charge Z) escaping a solid surface with velocity $v = dR/dt \ll 1$ a.u., where $R = vt$ is the instant ion-surface distance. We take into account both the active electron's initial state at the time $t = t_{in} = 0$ and the final state at the time $t = t_{fin} \to \infty$. In other words, we analyze a system that is "preselected" in the "metallic" parabolic state $|\mu_M\rangle$, where $\mu_M = (\gamma_M, n_{1M}, m_M)$ and "postselected" in the spherical "atomic" state $|\nu_A\rangle$, where $\nu_A = (n_A, l_A, m_A)$, and calculate the intermediate probabilities and rates for the neutralization process (see Fig. 1).

At the time $t \in (t_{in}, t_{fin})$ the state of the considered active electron is described by two state vectors. The first state evolves by the first scenario according to the law

$$|\Psi_1(t)\rangle = \hat{U}_1(t_{in}, t)|\mu_M\rangle. \tag{2.1}$$

The second state $|\Psi_2(t)\rangle$ evolves backward in time (by the second scenario) from the fixed final state according to the law

$$|\Psi_2(t)\rangle = \hat{U}_2(t_{fin}, t)|\nu_A\rangle. \tag{2.2}$$

By $\hat{U}_i(t_1, t_2)$, $i = 1, 2$, we denoted the evolution operators in the ith scenario. In the TVM applied in the present paper, the evolution operators $\hat{U}_1(t_{in}, t)$ and $\hat{U}_2(t_{fin}, t)$ are determined by the "in- and out-channel" Hamiltonians $\hat{H}_1$ and $\hat{H}_2$, respectively.

The one-electron Hamiltonians $\hat{H}_i$ outside the solid are given by

$$\hat{H}_i(R) = -\frac{1}{2}\nabla^2 + U_A^{(i)} + U_S^{(i)}, \quad i = 1, 2, \qquad (2.3)$$

where $U_A^{(i)}$ is the effective potential energy of the active electron in the field of the polarized ionic core. The surface potential $U_S^{(i)}$ in Eq. (2.3) is the electron potential energy in the field of the polarized solid.

The potentials that include the surface and ionic polarizations are not known exactly. There is a variety of "true" surface potentials $U_S^{(i)}$ which are finite at the surface and are smoothly connected with the bulk potential at the surface (see, for example, Refs. [1,7,9,14] and references therein). However, taking into account that the TVM is based on calculation of the mixed flux through the Firsov plane placed sufficiently far from the surface (see the Introduction), our model is almost independent of the form of the near-surface potential. Also, in the first approximation the dynamical response of the surface can be neglected. Due to this, it is sufficiently accurate to use the classical electrostatic image potentials; in the coordinate system with the origin at the surface and the z axis oriented along the ionic motion (perpendicular to surface), we have

$$U_S^{(i)} = U_M^{(i)} + U_{AM}^{(i)}, \quad z > 0, \qquad (2.4)$$

where $U_M^{(i)} = -1/(4z)$, and $U_{AM}^{(i)} = Z/\sqrt{\rho^2 + (z+R)^2}$, whereas $\rho^2 = x^2 + y^2$. At sufficiently large ion-surface distance ($R \gg 1$) and in the narrow cylindrical region around the z axis ($\rho \approx 0$), we have

$$U_S^{(i)} \approx -\frac{1}{4z} + \frac{Z}{z+R} \equiv U_S. \qquad (2.5)$$

In the vicinity of the ionic core ($z \approx R$) and for $\rho \ll R$, the expression for the surface potential can be further simplified:

$$U_S \approx \frac{2Z-1}{4R}. \qquad (2.6)$$

The interaction of the active electron with the polarized ionic core can also be expressed by different model potentials. For the bare nucleus, or at very large distances r_A between the active electron and projectile when it can be treated as a point charge (first scenario), $U_A^{(i)}$ is simply the Coulomb interaction:

$$U_A^{(1)} = -\frac{Z}{r_A}. \qquad (2.7)$$

In the second scenario the active electron moves closer to the charge cloud of the electrons already bound to the nucleus. In that case, the active electron interacts with the ion through the corresponding effective potential. For $r_A \gg 1$, the sufficiently accurate expression for $U_A^{(2)}$ is the Simons-Bloch potential [33]

$$U_A^{(2)} = -\frac{Z}{r_A} + \sum_{l'=0}^{\infty} \frac{c_{l'}}{r_A^2} \hat{P}_{l'}, \qquad (2.8)$$

where $\hat{P}_{l'} = |l'\rangle\langle l'|$ is the projection operator onto the subspace of a given angular momentum l'. The effective poten-

tial $U_A^{(2)}$ accounts for the experimentally observed quantum defects of the energy spectra $\widetilde{E}_A = -\widetilde{\gamma}_A^2/2$ through the constants $c_{l'}$. Using the expression (2.8), the eigenvalue problem of the Hamiltonian $\widetilde{H}_2 = -\nabla^2/2 + U_A^{(2)}$ can be solved exactly.

In the region inside the solid ($z < 0$), the in and out Hamiltonians are expressed by the following forms:

$$\hat{H}_1 = -\frac{1}{2}\nabla^2 - U_0, \quad \hat{H}_2 = -\frac{1}{2}\nabla^2 - \frac{Z}{r_A}, \qquad (2.9)$$

where U_0 is the depth of the potential well of the Sommerfeld model of the solid. The Coulomb interaction inside the solid in the second scenario is introduced for convenience. By the above two forms we take into account that the electron motion in the first scenario is infinite, and that the electronic state of the second scenario corresponds to the bound-state configuration.

We point out that the use of two scenarios has a practical advantage: the main effects of the polarization of the solid surface and the polarization of the ionic projectile, characterized by different symmetries, can be treated independently. That is, in the first scenario the dominant effect is the polarization of the solid surface, which pertain to parabolic symmetry, and in the second one the spherically symmetric polarization of the ionic core prevails.

B. The time-symmetrized description of neutralization

In order to describe intermediate stages of neutralization, we define the two-state probability amplitude [23]

$$A_{\mu_M,\nu_A}(t) = \langle\Psi_2(t)|\hat{P}_A(t)|\Psi_1(t)\rangle, \qquad (2.10)$$

where $\hat{P}_A(t) = \int_{V_A} |\vec{r}_A\rangle\langle\vec{r}_A| dV$ is the projection operator onto the ionic region V_A. The amplitude $A_{\mu_M,\nu_A}(t)$ satisfies the initial condition $A_{\mu_M,\nu_A}(t_{in}^*) = 0$, where $t_{in}^* > t_{in}$ is the time at which the neutralization begins. The intermediate neutralization probability per unit γ_M is given by

$$T_{\mu_M,\nu_A}(t) = |A_{\mu_M,\nu_A}(t)|^2. \qquad (2.11)$$

Taking into account the multielectron character of the process, the intermediate neutralization probability $P_{\nu_A}(t)$ is defined as the integral over the solid conduction band energy parameter γ_M and the sum over n_{1M} and m_M of the quantity $T_{\mu_M,\nu_A}(t)$:

$$P_{\nu_A}(t) = \int \sum_{n_{1M},m_M} T_{\mu_M,\nu_A}(t)d\gamma_M. \qquad (2.12)$$

The neutralization probability $T_{\mu_M,\nu_A}(t)$ per unit γ_M can be expressed via the mixed flux $I_{\mu_M,\nu_A}(t)$ through the surface $S_A(t)$ containing the ion, partially consists of the Firsov plane S_F positioned between the ion and the surface, i.e., for $t > t_{in}^*$ we get

$$T_{\mu_M,\nu_A}(t) = \left|\int_{t_{in}^*}^{t} I_{\mu_M,\nu_A}(t)dt\right|^2, \qquad (2.13)$$

where

$$I_{\mu_M,\nu_A}(t) = -\oint_{S_A(t)} (\vec{j}_{12} - \rho_{12}\vec{u}) \cdot d\vec{S}, \qquad (2.14)$$

where $\vec{u}$ is the velocity of the surface element $d\vec{S}$. The mixed flux is determined by the "two-amplitude" $\rho_{12}(\vec{r},t) = \Psi_1(\vec{r},t)\Psi_2^*(\vec{r},t)$ and the "two-current" density $\vec{j}_{12}(\vec{r},t) = (\Psi_2^*\vec{\nabla}\Psi_1 - \Psi_1\vec{\nabla}\Psi_2^*)/(2i)$; for the terminology, see Ref. [30]. Moreover, the neutralization dynamics is completely determined by the behavior of these quantities exclusively on the Firsov plane S_F, i.e., in the region of negligible ion-surface interaction.

The intermediate stages of the neutralization can be characterized by the normalized probability

$$\widetilde{P}_{\nu_A}(t) = \frac{P_{\nu_A}(t)}{P_{\nu_A}^{fin}}, \qquad (2.15)$$

where $P_{\nu_A}^{fin} = \lim_{t \to t_{fin}} P_{\nu_A}(t)$. The introduced probability $\widetilde{P}_{\nu_A}(t)$ tends to 1 for $t \to t_{fin}$, i.e., it is defined under the condition that the considered Rydberg state $|\nu_A\rangle$ is finally populated with certainty. The probability $\widetilde{P}_{\nu_A}(t)$ can be used for the calculation of the corresponding neutralization rate

$$\widetilde{\Gamma}_{\nu_A}(t) = \frac{d\widetilde{P}_{\nu_A}(t)}{dt}. \qquad (2.16)$$

The kinematics of the Firsov plane is determined by the variational requirement

$$\frac{\delta\widetilde{P}_{\nu_A}(t)}{\delta a(t)} = 0, \qquad (2.17)$$

where $a = a(t)$ is the position of the S_F plane with respect to the ion: $z_A = -a$. Equation (2.17) reflects the fact that the probability $\widetilde{P}_{\nu_A}(t)$ should be independent of the small variations of the S_F plane position.

We point out that the rates $\widetilde{\Gamma}_{\nu_A}(t)$, with $a = a(t)$ obtained from Eq. (2.17), are directly related to the problem of localization of the neutralization process. That is, the maxima of the rates $\widetilde{\Gamma}_{\nu_A}(t)$ determine the neutralization distances R_c^N [22] for the process $A^{Z+} + M(e) \to A^{(Z-1)+} + M$ in which the electron e is in a given Rydberg state $|\nu_A\rangle$ for $t \to t_{fin}$.

III. THE MIXED FLUX AND INTERMEDIATE PROBABILITY

A. The functions $\Psi_1(\vec{r},t)$ and $\Psi_2(\vec{r},t)$

The electron capture into Rydberg states of multiply charged Rydberg ions occurs at large ion-surface distances R, and all our calculations are performed on the Firsov plane, which is sufficiently far from the surface as well as from the ionic core. Therefore, it is possible to apply the appropriate asymptotic methods in the calculation of the functions $\Psi_1(\vec{r},t)$ and $\Psi_2(\vec{r},t)$.

In order to obtain the functions $\Psi_1(\vec{r},t)$ and $\Psi_2(\vec{r},t)$, first we consider the eigenvalue problems of the Hamiltonians $\hat{H}_1$

and $\hat{H}_2$ at a given ion-surface separation R. The Hamiltonian $\hat{H}_1$ describes the parabolically symmetric system; it can be completed by the Runge-Lenz operator $\hat{A}_z$ and the operator $\hat{L}_z$, where $\hat{\vec{L}}$ is the orbital angular momentum operator. The energy spectrum of $\hat{H}_1$ is continuous: $E_M = -\gamma_M^2/2$, where γ_M is the continuous energy parameter; the corresponding eigenfunctions will be denoted by Φ_{MA,μ_M}. On the other hand, the Hamiltonian $\hat{H}_2$ describes the spherically symmetric ion-surface system, i.e., the operators $\hat{H}_2$, $\hat{L}^2$, and $\hat{L}_z$ constitute the complete set of observables. The operator $\hat{H}_2$ has a discrete spectrum $E_A = -\gamma_A^2/2$ with the eigenfunctions Φ_{AM,ν_A}. Hence,

$$\hat{H}_1\Phi_{MA,\mu_M} = -\frac{\gamma_M^2}{2}\Phi_{MA,\mu_M}, \qquad (3.1a)$$

$$\hat{H}_2\Phi_{AM,\nu_A} = -\frac{\gamma_A^2}{2}\Phi_{AM,\nu_A}. \qquad (3.1b)$$

In the vicinity of the Firsov plane, the wave function Φ_{MA,μ_M} exponentially decreases in the direction from the metal (M) to the ionic core (A). On the other hand, the wave function Φ_{AM,ν_A} behaves as an exponentially decreasing function in the direction $A \to M$. In the solid region, these two functions have the following behaviors: the function Φ_{MA,μ_M} represents the sum of the incoming and outgoing waves with respect to the surface, while the function Φ_{AM,ν_A} is negligible.

The eigenvalue problem (3.1a) can be solved in the region of dominant electron transitions (the narrow cylindrical region around the z axis) by the method of separation of variables in the parabolic coordinates $\xi = r_A + z_A$, $\eta = r_A - z_A$, φ_A, taking that $\Phi_{MA,\mu_M} = X(\xi)Y(\eta)e^{im_M\varphi_A}/\sqrt{\xi\eta}$. The effective eigenvalue problem along the ξ direction reduces to Whittaker's differential equation, so that the solution $X(\xi)$ can be expressed in terms of Whittaker's function $M_{\lambda,\tau}(x)$. However, the eigenvalue problem along the η axis can be solved only approximately; a suitable method for obtaining a sufficiently accurate eigenfunction $Y(\eta)$ is the Jeffreys-Wentzel-Kramers-Brillouin (JWKB) method [34].

The function $X(\xi)$ that satisfies the condition $X(0) = X(\infty) = 0$ is given by

$$X(\xi) = M_{-\mathcal{L}/\gamma_M, m_M/2}(\gamma_M\xi), \qquad (3.2)$$

where $-\mathcal{L}/\gamma_M = n_{1M} + (m_M + 1)/2$. Furthermore, taking into account that the condition $\xi \approx 0$ is satisfied in the vicinity of the z axis, the Whittaker function in expression (3.2) can be significantly simplified. The solutions $Y(\eta)$ inside the solid ($\eta > 2R$) and in the vicinity of the Firsov plane ($z_A \approx -a$, $\eta \approx 2a$) are given by the following expressions:

$$Y(\eta) = K^{(1)}W_{\mathcal{L}/i\kappa_M, m_M/2}(i\kappa_M\eta) + K^{(2)}W_{-\mathcal{L}/i\kappa_M, m_M/2}(-i\kappa_M\eta),$$
$$(3.3a)$$

$$Y(\eta) = K M_{(Z+\mathcal{L})/\gamma_M, m_M/2}(\gamma_M \eta), \qquad (3.3b)$$

respectively, where $M_{\lambda,\tau}(x)$ and $W_{\lambda,\tau}(x)$ are Whittaker's functions, and $\kappa_M = \sqrt{2U_0 - \gamma_M^2}$. For sufficiently large ion-surface distances R, i.e., $\gamma_M R \gg 1$, the solutions (3.3a) and (3.3b) can be connected through the barrier within the framework of the JWKB method [35]. In that way, under the condition $K^{(2)} = \exp(i\Delta)K^{(1)}$, we get the relation between the constants K and $K^{(1)}$; the remaining unknown constant K can be obtained from the normalization condition $\langle \Phi_{MA,\mu_M} | \Phi_{MA,\mu'_M} \rangle = \delta(\gamma_M - \gamma'_M)$. We point out that the ambiguous surface potential U_S in the near-surface region $\eta \approx 2R$ appears only in the unimportant phase factor Δ.

The function Φ_{MA,μ_M} in the vicinity of the Firsov plane can be expressed as

$$\Phi_{MA,\mu_M} = D_M Q_{\mu_M}(R) \frac{\xi^{m_M/2}}{\sqrt{\eta}} e^{-\gamma_M \xi/2}$$
$$\times M_{Z/\gamma_M - n_{1M} - (m_M+1)/2, m_M/2}(\gamma_M \eta) e^{im_M \varphi_A}, \qquad (3.4)$$

where, up to a phase factor,

$$D_M = \frac{1}{\pi} \left(\frac{(n_{1M} + m_M)!}{2 n_{1M}!} \right)^{1/2}$$
$$\times \frac{\Gamma(-Z/\gamma_M + m_M + 1 + n_{1M})}{(m_M!)^2} \gamma_M^{Z/\gamma_M + (m_M+1)/2}$$
$$\times (2\gamma_M)^{1/2 \gamma_M - n_{1M} - (m_M+1)/2}(2e)^{1/4 \gamma_M}. \qquad (3.5)$$

By Q_{μ_M} we denoted the following R-dependent quantity:

$$Q_{\mu_M}(R) = R^{Z/\gamma_M - n_{1M} - (m_M+1)/2 + 1/4 \gamma_M} e^{-\gamma_M R}. \qquad (3.6)$$

The eigenvalue problem of the Hamiltonian $\tilde{\hat{H}}_2 = -\nabla^2/2 + U_A^{(2)}$ of an ion with a polarized core (with eigenenergies $\tilde{E}_A = -\tilde{\gamma}_A^2/2$ and eigenfunctions $\tilde{\Phi}_{AM,\nu_A}$) can be solved exactly, i.e., the eigenfunctions can be expressed in terms of Whittaker's function $M_{\lambda,\tau}(x)$ and spherical harmonics. The full Hamiltonian $\hat{H}_2$ of the second scenario is defined by $\hat{H}_2 = \tilde{\hat{H}}_2 + U_S$. In the first approximation, the surface potential U_S of the polarized solid is given by Eq. (2.6). In this approximation, for the eigenenergies of the Hamiltonian $\hat{H}_2$ we get

$$E_A(R) = -\frac{\gamma_A^2}{2} = -\frac{\tilde{\gamma}_A^2}{2} + \frac{2Z-1}{4R}; \qquad (3.7)$$

in the same approximation we have $\Phi_{AM,\nu_A} = \tilde{\Phi}_{AM,\nu_A}$. The solid polarization in the second scenario can be taken into account more exactly, using the value γ_A instead of $\tilde{\gamma}_A$ in the function $\tilde{\Phi}_{AM,\nu_A}$. This procedure is consistent with the further calculation of the wave function Ψ_2. We point out that the proposed expression for the eigenfunction Φ_{AM,ν_A} is somewhat different from the corresponding expression used in the intermediate-velocity case [21,22].

According to the above considerations, the eigenfunction Φ_{AM,ν_A} of the Hamiltonian $\hat{H}_2$ for the electron in the field of the polarized ionic core and polarized solid is given by

$$\Phi_{AM,\nu_A} = \frac{D_A}{r_A} M_{Z/\tilde{\gamma}_A, \tilde{l}_A + 1/2}(2\gamma_A r_A) Y_{l_A m_A}(\theta_A, \varphi_A), \qquad (3.8)$$

where the spherical harmonics $Y_{l_A m_A}(\theta_A, \varphi_A)$ are expressed via the associated Legendre functions $P_{l_A}^{m_A}$ by the following relation:

$$Y_{l_A m_A}(\theta_A, \varphi_A) = N_{l_A m_A} P_{l_A}^{m_A}(\cos \theta_A) e^{im_A \varphi_A}, \qquad (3.9a)$$

$$N_{l_A m_A} = (-1)^{m_A} \left(\frac{(2l_A+1)(l_A - m_A)!}{4\pi(l_A + m_A)!} \right)^{1/2}. \qquad (3.9b)$$

The constant D_A in Eq. (3.8), obtained from the normalization condition $\langle \Phi_{AM,\nu_A} | \Phi_{AM,\nu_A} \rangle = 1$, is given by

$$|D_A| = \left(\frac{2\gamma_A(\tilde{l}_A + 1)(2\tilde{l}_A + 2)_{n_A - l_A - 1}}{(n_A + \tilde{l}_A - l_A)(n_A - l_A - 1)!\, \Gamma(2\tilde{l}_A + 3)} \right)^{1/2}. \qquad (3.10)$$

The energy parameter γ_A is expressed via the parameter $\tilde{\gamma}_A = Z/\tilde{n}_A$ by Eq. (3.7). The quantity $\tilde{\gamma}_A$ can be obtained from the experimentally known spectra ($E_{expt} = \tilde{E}_A = -\tilde{\gamma}_A^2/2$). The modified angular momentum quantum number $\tilde{l}_A$ is defined by

$$\tilde{l}_A = l_A + \tilde{n}_A - n_A. \qquad (3.11)$$

The quantity $\tilde{l}_A$ can also be expressed in terms of the coefficients c_l of the Simons-Bloch potential model (2.8) by the following relation: $\tilde{l}_A = \sqrt{(l_A + 1/2)^2 + 2c_l} - 1/2$; for pointlike core charges ($c_l \to 0$) we have $\tilde{l}_A \to l_A$ and $\tilde{n}_A \to n_A$, i.e., $\tilde{E}_A \to E_A^{(0)} = -\gamma_{A0}^2/2$ where $\gamma_{A0} = Z/n_A$. We point out that for $\tilde{n}_A = Z/\tilde{\gamma}_A$ obtained from experimental spectra, the model coefficients $c_l = (\tilde{n}_A - n_A)(\tilde{n}_A - n_A + 2l_A + 1)/2$ depend not only on l_A but also on n_A, so that we have a form of self-consistent interaction of the active electron and the ionic core.

The wave functions $\Psi_1(t)$ and $\Psi_2(t)$ can be expressed as space-time modifications of the eigenfunctions Φ_{MA,μ_M} and Φ_{AM,ν_A} [21,22]:

$$\Psi_1(\vec{r}, t) = \Phi_{MA,\mu_M} \exp\left(f_M + \frac{i\gamma_M^2 t}{2} \right), \qquad (3.12a)$$

$$\Psi_2(\vec{r}, t) = \Phi_{AM,\nu_A} \exp\left(ivz - \frac{iv^2 t}{2} \right) \exp\left(f_A + \frac{i\gamma_A^2 t}{2} \right). \qquad (3.12b)$$

By $f_M = f_M(\vec{r}, t)$ and $f_A = f_A(\vec{r}, t)$ we denoted the corresponding correction factors, whereas $\exp(ivz - iv^2 t/2)$ represents the Galilei factor. The functions f_M and f_A follow from the time-dependent Schrödinger equations of the first and second scenarios, respectively. The factor f_M that satisfies the initial

condition $f_M(\vec{r},t) \to 0$ when $t \to t_{in}=0$ and $a/R \to 1$ is given by [21]

$$f_M = Z\left(\frac{1}{\gamma_M} - \frac{1}{\gamma_M + iv}\right)\ln\left(\frac{a}{R}\right)$$
$$+ Z\left(\frac{1}{\gamma_M} - \frac{1}{\gamma_M - iv}\right)\ln\left(2 - \frac{a}{R}\right). \quad (3.13)$$

On the other hand, for the factor f_A, calculated with the "exact" expression for U_S, Eq. (2.5), along with the final condition $f_A(\vec{r}_A,t) \to 0$ when $t=t_{fin} \to \infty$ and $a/R \to 0$, we get

$$f_A = -\frac{(2Z-1)}{4\tilde{\gamma}_A}\frac{a}{R} + \frac{1}{4}\left(\frac{1}{\tilde{\gamma}_A} - \frac{1}{\tilde{\gamma}_A + iv}\right)\ln\left(1 - \frac{a}{R}\right)$$
$$- Z\left(\frac{1}{\tilde{\gamma}_A} - \frac{1}{\tilde{\gamma}_A + 2iv}\right)\ln\left(1 - \frac{a}{2R}\right). \quad (3.14)$$

For a pointlike ionic core ($\tilde{\gamma}_A \to \gamma_{A0}$) from Eq. (3.14) we obtain the corresponding expression in Ref. [21].

Equations (3.12a) and (3.12b), in which the eigenfunctions Φ_{MA,μ_M} and Φ_{AM,ν_A} are given by Eqs. (3.4) and (3.8), and the space-time correction factors f_M and f_A are given by Eqs. (3.13) and (3.14), complete the two-state vector description of the electron state at the time $t \in (t_{in}, t_{fin})$. The wave functions $\Psi_1(\vec{r},t)$ and $\Psi_2(\vec{r},t)$ evolve in two opposite directions of time, from the given initial and final states, respectively. For $t=t_{in}$ and $t=t_{fin}$, these functions are characterized by the energy parameters $\gamma_{M,in}$ and $\gamma_{A,fin}$ of the initially occupied energy level of the solid and the postselected ionic state. At intermediate stages, the dynamical correlation with all conduction band states and all ionic states is included in the wave functions $\Psi_1(\vec{r},t)$ and $\Psi_2(\vec{r},t)$ via f_M and f_A. However, for sufficiently small f_M and f_A, the time evolutions of the wave functions $\Psi_1(\vec{r},t)$ and $\Psi_2(\vec{r},t)$ are quasistationary: the functions behave as eigenfunctions, with the energy parameters $\gamma_M = \gamma_{M,in} + O(1/R^2)$ and $\gamma_A = \sqrt{\tilde{\gamma}_A^2 - (2Z-1)/(2R)} + O(1/R^2)$, Eq. (3.7). Therefore, for sufficiently large R, with accuracy of $O(1/R^2)$, the values of the parameter γ_M remain within the initially occupied conduction band of the solid and the parameter γ_A increases with increasing R toward the value $\gamma_{A,fin} = \tilde{\gamma}_A$.

B. The mixed flux and the probability $T_{\mu_M,\nu_A}(t)$

All relevant physical quantities associated with the intermediate stages of the time-symmetrized description of neutralization can be expressed via the mixed flux $I_{\mu_M,\nu_A}(t)$, Eq. (2.14).

Therefore, it is necessary to calculate the following surface integral [21]:

$$I_{\mu_M,\nu_A}(t) = \frac{i}{2}\int_{S_F}\left[\frac{\vec{\nabla}\Psi_1}{\Psi_1} - \frac{\vec{\nabla}\Psi_2^*}{\Psi_2^*} - 2iv\left(1 - \frac{da}{dR}\right)\vec{e}_z\right]$$
$$\times \Psi_2^*(\vec{r},t)\Psi_1(\vec{r},t) \cdot d\vec{S}, \quad (3.15)$$

where S_F is the Firsov plane ($z_A=-a$). Taking into account the localization of the S_F plane in the asymptotic region

($z \gg 1$, $r_A \gg 1$) we get $\vec{\nabla}\Psi_1/\Psi_1 \approx -\gamma_M \vec{e}_z$ and $\vec{\nabla}\Psi_2^*/\Psi_2^* \approx -\gamma_A \vec{e}_{r_A} - iv\vec{e}_z$. With the former two expressions, the mixed flux can be expressed in the following form:

$$I_{\mu_M,\nu_A}(t) = \frac{i}{2}\exp(iwt)\left[\gamma_M + \gamma_A + iv\left(1 - 2\frac{da}{dR}\right)\right]$$
$$\times \exp(f_A^* + f_M)\int_{S_F}\Phi_{AM,\nu_A}^*\Phi_{MA,\mu_M}dS, \quad (3.16)$$

where

$$w = \frac{1}{2}(\gamma_M^2 - \gamma_A^2) - \frac{v^2}{2}\left(1 - 2\frac{a}{R}\right). \quad (3.17)$$

For further calculations it is convenient to express the mixed flux as follows:

$$I_{\mu_M,\nu_A}(t) = I_{\mu_M,\nu_A}^{(0)}(t)\mathcal{I}_{\mu_M,\nu_A}(R), \quad (3.18)$$

where

$$I_{\mu_M,\nu_A}^{(0)}(t) = i\pi\exp(iwt)\left[\gamma_M + \gamma_A + iv\left(1 - 2\frac{da}{dR}\right)\right]$$
$$\times \exp(f_A^* + f_M)D_A^* D_M Q_{\mu_M}(R)N_{l_A m_A}^* \delta_{m_A,m_M}, \quad (3.19)$$

whereas

$$\mathcal{I}_{\mu_M,\nu_A}(R) = \int_0^\infty \frac{\rho}{r_A}\frac{\xi^{m_M/2}}{\sqrt{\eta}}e^{-\gamma_M\xi/2}P_{l_A}^{m_A}(\cos\theta_A)$$
$$\times M_{Z/\tilde{\gamma}_A,\tilde{l}_A+1/2}(2\gamma_A r_A)$$
$$\times M_{Z/\gamma_M - n_{1M} - (m_M+1)/2, m_M/2}(\gamma_M\eta)d\rho. \quad (3.20)$$

In Eq. (3.20) we have $r_A = \sqrt{\rho^2 + a^2}$, while $\xi = r_A - a$, $\eta = r_A + a$ and $\cos\theta_A = z_A/r_A = -a/r_A$. The mixed flux $I_{\mu_M,\nu_A}(t)$ depends explicitly on the time t via the factor $\exp(iwt)$, and implicitly via $R=vt$, $\gamma_A = \gamma_A(R)$, $a=a(R)$, and $w=w(R)$.

In the calculation of the mixed flux we take into account that in the vicinity of the Firsov plane we have $2\gamma_A r_A \gg 1$ and $\gamma_M\eta = \gamma_M(r_A + a) \gg 1$, so that we can use the asymptotic expressions for both Whittaker's functions appearing in Eq. (3.20). Furthermore, in the low-velocity case considered in the present paper, the electron transitions are quasiresonant, i.e., $\gamma_A(R) \approx \gamma_M$. Under this condition, considering that the main contribution to the neutralization is given by the metallic electrons with $n_{1M} \approx 0$, and $m_M = m_A = 0$, as well as that our consideration is restricted to the ionic states with large eccentricities (low-l_A states), the integral $\mathcal{I}_{\mu_M,\nu_A}$ can be expressed by the following approximate form:

$$\mathcal{I}_{\mu_M,\nu_A}(R) = \frac{\Gamma(2\tilde{l}_A + 2)}{\Gamma(\tilde{l}_A + \tilde{n}_A + 1)}\frac{e^{i\pi(n_A-1)}}{\Gamma(-Z/\gamma_M + n_{1M} + 1)}$$
$$\times \gamma_A^{Z/\tilde{\gamma}_A - 1}\gamma_M^{-Z/\gamma_M + n_{1M} + 1/2}$$
$$\times (2a)^{Z/\tilde{\gamma}_A - Z/\gamma_M + n_{1M}}e^{-(\gamma_A - \gamma_M)a}. \quad (3.21)$$

We point out that the position of the Firsov plane depends on

R, i.e., $a = a(R) = gR$, where $g \approx$ const (see Sec. III C). For that reason, we have $\exp(-\gamma_A a) = \exp(-\gamma_A gR)$ $\approx \exp(-\tilde{\gamma}_A gR)\exp[(2Z-1)g/(4\tilde{\gamma}_A)]$.

The neutralization probability $T_{\mu_M,\nu_A}(t)$ per unit γ_M follows from Eq. (2.13), in which the mixed flux $I_{\mu_M,\nu_A}(t)$ is integrated over time from $t = t_{in}^*$ to t. The time t_{in}^* corresponds to the minimal ion-surface distance at which the neutralization process is energetically possible. In the case of quasiresonant neutralization, the quantity R_{in}^* can be defined by the condition $E_A = -\tilde{\gamma}_A^2/2 + (2Z-1)/(4R) = -\phi$, where ϕ is the solid work function, i.e.,

$$R_{in}^* = \frac{(2Z-1)}{2(\tilde{\gamma}_A^2 - 2\phi)}. \qquad (3.22)$$

Within the framework of the asymptotic methodology used throughout the paper, considering exclusively the normalized neutralization probability $\tilde{P}_{\nu_A}(t)$ and for the Rydberg states $n_A \approx Z \gg 1$, $l_A \ll n_A$, and $m_M = m_A = 0$, we get

$$T_{\mu_M,\nu_A}(t) \approx C_{\mu_M,\nu_A}(R)\left|1 - \left(\frac{R}{R_{in}^*}\right)^{\tilde{\alpha}} e^{-\beta(R-R_{in}^*)}\right|^2, \qquad (3.23)$$

where $C_{\mu_M,\nu_A}(R)$, depending weakly on R via γ_A, is given by

$$
\begin{aligned}
C_{\mu_M,\nu_A}(R) = {} & \frac{(2l_A+1)}{8\pi v^2} \frac{\Gamma(2\tilde{l}_A+2)}{\Gamma^2(\tilde{l}_A+\tilde{n}_A+1)} \frac{(2\tilde{l}_A+2)_{n_A-l_A-1}}{(n_A+\tilde{l}_A-l_A)(n_A-l_A-1)!} \gamma_A^{2Z/\tilde{\gamma}_A-1} 2^{1/\gamma_M-2n_{1M}-1} \gamma_M^{1/\gamma_M+1}(2e)^{1/2\gamma_M} \\
& \times [g(2-g)]^{2Zv^2/\gamma_M(\gamma_M^2+v^2)}(1-g)^{v^2/2\tilde{\gamma}_A(\tilde{\gamma}_A^2+v^2)}\left(1 - \frac{g}{2}\right)^{-8Zv^2/\tilde{\gamma}_A(\tilde{\gamma}_A^2+4v^2)} \\
& \times (2g)^{2Z/\tilde{\gamma}_A-2Z\gamma_M+2n_{1M}} \frac{(\gamma_M+\gamma_A)^2 + v^2(1-2g)^2}{\tilde{\beta}^2 + w^2/v^2} R_{in}^{*2\tilde{\alpha}} e^{-2\tilde{\beta}R_{in}^*}.
\end{aligned}
\qquad (3.24)
$$

In the above expressions, we introduced the quantities α and β as in Ref. [21], as well as the quantities $\tilde{\alpha}$ and $\tilde{\beta}$, by the following expressions:

$$\alpha = \frac{Z}{\tilde{\gamma}_A} - \frac{3}{2} + \frac{1}{4\gamma_M} \equiv \tilde{\alpha} - 1, \qquad (3.25a)$$

$$\beta = \gamma_M + (\tilde{\gamma}_A - \gamma_M)g - i\frac{w}{v} \equiv \tilde{\beta} - i\frac{w}{v}. \qquad (3.25b)$$

On the basis of Eq. (3.23), we obtain the following properties of the quantity $T_{\mu_M,\nu_A}(t)$ for $t = t_{in}^*$ and $t = t_{fin}$:

$$\lim_{t \to t_{in}^*} T_{\mu_M,\nu_A}(t) = 0, \qquad (3.26a)$$

$$\lim_{t \to t_{fin}} T_{\mu_M,\nu_A}(t) = T_{\mu_M,\nu_A}^{fin} = C_{\mu_M,\nu_A}(R)/_{\gamma_A \to \tilde{\gamma}_A}. \qquad (3.26b)$$

Due to the factor $\exp[i(w/v)(R-R_{in}^*)]$ in Eq. (3.23), the quantity $T_{\mu_M,\nu_A}(t)$ approaches the final value T_{μ_M,ν_A}^{fin} in the oscillatory regime, characteristic for interference effects. Also, the γ_M dependence of the probability density $T_{\mu_M,\nu_A}(t)$ is rather complicated and changes with the ion-surface distance R.

C. The normalized intermediate probabilities and rates

The intermediate probability $P_{\nu_A}(t)$, Eq. (2.12), for the considered Rydberg ion being partially neutralized at the distance R from surface (under a fixed final condition) can be obtained by integration of the quantity $T_{\mu_M,\nu_A}(t)$ over all possible values of the energy parameter $\gamma_M \in [\gamma_\phi = \sqrt{2\phi}, \gamma_U = \sqrt{2U_0}]$ of the solid, and performing the summation over n_{1M} and m_M. In the low-velocity case, considered in the present paper, we get

$$P_{\nu_A}(t) \approx \left|1 - \left(\frac{R}{R_{in}^*}\right)^{\tilde{\alpha}} e^{-\beta(R-R_{in}^\star)}\right|^2_{\gamma_M=\gamma_{max}}$$

$$\times \int_{\gamma_\phi}^{\gamma_U} \sum_{n_{1M}} C_{\mu_M,\nu_A}(R)d\gamma_M, \qquad (3.27)$$

where γ_{max} is the energy parameter of the solid which gives the main contribution to the neutralization at a given R and $m_M = m_A = 0$. The quantity γ_{max} can be determined from the position of maximum of the quantity $C_{\mu_M,\nu_A}(R)$ with respect to γ_M. In deriving the expression (3.27) it was assumed that γ_{max} is independent of n_{1M}.

The probability $\tilde{P}_{\nu_A}(t)$ is defined by Eq. (2.15) as a ratio of $P_{\nu_A}(t)$ and $P_{\nu_A}^{fin}$, where

$$P_{\nu_A}^{fin} = \lim_{t \to t_{fin}} P_{\nu_A}(t) \approx \int_{\gamma_\phi}^{\gamma_U} \sum_{n_{1M}} C_{\mu_M,\nu_A}(R)/_{\gamma_A \to \tilde{\gamma}_A} d\gamma_M. \qquad (3.28)$$

Therefore, taking into account that $\int \sum C_{\mu_M,\nu_A}d\gamma_M \approx \int \sum C_{\mu_M,\nu_A}/_{\gamma_A \to \tilde{\gamma}_A}d\gamma_M$, we obtain

$$\widetilde{P}_{\nu_A}(t) \approx \left| 1 - \left(\frac{R}{R_{in}^*} \right)^{\tilde{\alpha}} e^{-\beta(R-R_{in}^*)} \right|^2, \qquad (3.29)$$

i.e.,

$$\widetilde{P}_{\nu_A}(t) = \left[1 + f^2(R) - 2f(R)\cos\left(\frac{w}{v}(R - R_{in}^*) \right) \right], \qquad (3.30)$$

where

$$f(R) = \left(\frac{R}{R_{in}^*} \right)^{\tilde{\alpha}} e^{-\tilde{\beta}(R-R_{in}^*)} \qquad (3.31)$$

and $\gamma_M = \gamma_{max}$. According to Eqs. (3.23) and (3.29), the probability density $T_{\mu_M,\nu_A}(t)$ can be expressed in the following form:

$$T_{\mu_M,\nu_A}(t) \approx C_{\mu_M,\nu_A}(R)\widetilde{P}_{\nu_A}(t). \qquad (3.32)$$

The quantity $T_{\mu_M,\nu_A}(t)$ represents the product of the probability $\widetilde{P}_{\nu_A}(t)$, defined for a fixed final electronic state, and the quantity $C_{\mu_M,\nu_A}(R)$, in which the initial and final conditions are mixed and which is weakly dependent on the time.

The dependence of $\widetilde{P}_{\nu_A}(t)$ on the Firsov plane position $a = gR$ can be minimized using the variational requirement (2.17) for the factor g: $\delta\widetilde{P}_{\nu_A}(t)/\delta g = 0$. Inserting Eq. (3.30) in the last condition, we obtain

$$-(\tilde{\gamma}_A - \gamma_M)f(R) + (\tilde{\gamma}_A - \gamma_M)\cos\left(\frac{w}{v}(R - R_{in}^*) \right)$$

$$+ v\sin\left(\frac{w}{v}(R - R_{in}^*) \right) = 0. \qquad (3.33)$$

The above equation reduces to the conditions $w=0$ and $\tilde{\gamma}_A = \gamma_M$. From the condition $w=0$, for $\gamma_M \approx \gamma_A$, we get

$$g = \frac{1}{2}\left(1 + \frac{\gamma_A^2 - \gamma_M^2}{v^2} \right) = \frac{1}{2}, \qquad (3.34)$$

meaning that the Firsov plane is positioned at the half distance between the ionic core and the solid surface. We note that the value $g=1/2$ is obtained with the expression (3.30) for $\widetilde{P}_{\nu_A}(t)$ valid in the region $R \approx R_c^N$, most relevant for the neutralization process. On the other hand, the space-time correction factors f_M and f_A were obtained under the conditions: $g = a/R \rightarrow 1$ for $R \rightarrow R_{in} = 0$ and $g = a/R \rightarrow 0$ for $R \rightarrow R_{fin} \rightarrow \infty$.

With the known expression for g, the probability $\widetilde{P}_{\nu_A}(t)$ can be calculated from Eq. (3.30). The corresponding rate $\widetilde{\Gamma}_{\nu_A}(t) = d\widetilde{P}_{\nu_A}(t)/dt$ is given by

$$\widetilde{\Gamma}_{\nu_A}(t) = 2vf(R)\left\{ \left(\frac{\tilde{\alpha}}{R} - \tilde{\beta} \right)\left[f(R) - \cos\left(\frac{w}{v}(R - R_{in}) \right) \right] \right.$$

$$\left. + \frac{w}{v}\sin\left(\frac{w}{v}(R - R_{in}) \right) \right\}_{\gamma_M = \gamma_{max}}. \qquad (3.35)$$

Equations (3.30) and (3.35) completely determine the probability $\widetilde{P}_{\nu_A}(t)$ and rate $\widetilde{\Gamma}_{\nu_A}(t)$, respectively, providing that the

value γ_{max} is known. The variational requirement $\delta\widetilde{P}_{\nu_A}(t)/\delta g = 0$ leads to the quasiresonant condition $\gamma_{max} = \gamma_A(R)$. In the next section we shall demonstrate that the same condition follows from the very definition of γ_{max}.

The neutralization distances R_c^N can be obtained on the bases of the neutralization rates $\widetilde{\Gamma}_{\nu_A}(t)$ from the following condition [22]:

$$\left(\frac{d\widetilde{\Gamma}_{\nu_A}(t)}{dt} \right)_{R=R_c^N} = 0. \qquad (3.36)$$

We point out that, taking the quantity $T_{\mu_M,\nu_A}(t)$ into consideration, the following, more general, problem can be formulated: if the electron is initially in the metal in the state $|\mu_M\rangle$, and finally is found bounded to the ion in the given Rydberg state $|\nu_A\rangle$, where does the charge exchange take place? In the present paper, we restrict the problem, by considering the neutralization distances for the fraction of ions with a given final state $\nu_A = (n_A, l_A, m_A)$, but with an arbitrary initial state μ_M; thus the neutralization distances R_c^N defined by Eq. (3.36) depend only on ν_A.

We also point out that the multichannel character of the neutralization, which is manifested in the stepwise neutralization with formation of hollow atoms, has a different connotation within the framework of the TVM; namely, the quantum ensemble describing the intermediate stages of the process is formed only of ions with populated Rydberg states $\nu_A = (n_A, l_A, m_A)$ at $t \rightarrow t_{fin}$.

IV. RESULTS

A. Determination of γ_{max} and explicit expressions for $\widetilde{P}_{\nu_A}(t)$ and $\widetilde{\Gamma}_{\nu_A}(t)$

We apply the TVM developed in the present paper to the ions Ar VIII, Kr VIII, and Xe VIII characterized by the same value of core charge $Z=8$, but with different core polarizations.

The relevant values of $\tilde{\gamma}_A = \sqrt{-2\widetilde{E}_A}$ calculated according to Ref. [36] are given in Table I. The presented data correspond to the ground-state configuration of the ionic core with zero angular momentum and spin, i.e., the total orbital angular momentum of the considered Rydberg ions is $L = l_A$ and spin $S = 1/2$; the data in Table I are for minimal total angular momentum $J = |l_A - 1/2|$.

We begin the analysis of the results obtained with determination of the energy parameter $\gamma_M = \gamma_{max}$, which gives the main contribution to the neutralization process at a given R. The values γ_{max} can be obtained from the γ_M behavior of $T_{\mu_M,\nu_A}(t) \sim C_{\mu_M,\nu_A}(R)$. For $g=1/2$ and $w = (\gamma_M^2 - \gamma_A^2)/2$, we have

$$T_{\mu_M,\nu_A}(t) = T_{\nu_A}^{(0)}(t)2^{1/\gamma_M}\gamma_M^{1/\gamma_M+1}(2e)^{1/2\gamma_M}\left(\frac{3}{4} \right)^{2Zv^2/\gamma_M(\gamma_M^2+v^2)}$$

$$\times \frac{(\gamma_M + \gamma_A)^2}{\tilde{\beta}^2 + w^2/v^2} R_{in}^{*\,1/2\gamma_M}e^{-\gamma_M R_{in}^*}, \qquad (4.1)$$

where $T_{\nu_A}^{(0)}(t)$ is independent of γ_M. Taking into account that

TABLE I. Energy parameter $\tilde{\gamma}_A$ (a.u.) for the ions Ar VIII, Kr VIII, and Xe VIII, and the values $\gamma_{A0} = Z/n_A$ (a.u.).

n_A	$l_A=0$	$l_A=1$	$l_A=2$	$l_A=3$	γ_{A0}
Ar VIII					
6	1.459	1.414	1.354	1.335	1.333
7	1.235	1.202	1.158	1.146	1.143
8	1.069	1.046	1.012	1.002	1.000
9	0.941	0.925	0.897	0.889	0.889
10	0.885	0.829	0.807	0.802	0.800
11		0.750	0.735	0.725	0.727
12		0.672	0.667		0.667
Kr VIII					
6	1.714	1.638	1.497	1.353	1.333
7	1.411	1.358	1.260	1.160	1.143
8	1.198	1.160	1.088	1.011	1.000
9	1.043	1.015	0.959	0.899	0.889
Xe VIII					
6	2.045	1.936	1.727	1.474	1.333
7	1.626	1.555	1.416	1.244	1.143
8	1.349	1.297	1.202	1.077	1.000
9	1.156	1.117	1.045	0.950	0.889

the position of the maximum of the above function determines the value γ_{max}, we conclude that γ_{max} depends on R (via γ_A), the principal quantum number n_A, the orbital quantum number l_A, the core charge Z, and the velocity v; γ_{max} is independent of n_{1M}, which was assumed in Eq. (3.27).

In Fig. 2 the quantity $T_{\mu_M,\nu_A}/T_{\mu_M,\nu_A}^{max}$ as a function of the energy parameter γ_M for the neutralization of the Ar^{8+} ions escaping the solid surface with velocity $v=0.01$ a.u. is presented. In Figs. 2(a)–2(c) we consider the population of the Rydberg states of Ar VIII ion with the principal quantum numbers $n_A=6,8$, and 10, respectively, orbital quantum number $l_A=0$ and $m_A=0$, for the following characteristic ion-surface distances: $R=R_{in}^*$, $R=R_{in}^*+\Delta R$ for $\Delta R=5$ a.u., and $R=R_{fin} \rightarrow \infty$. The full and dashed curves correspond to the cases with and without polarization of the ionic core, respectively. The energy parameter γ_M varies from γ_ϕ (Fermi level) to γ_U; in Fig. 2 we consider the Al surface with $\phi \approx 5$ eV and $U_0 \approx 15$ eV. The bounds of the solid conduction band are marked by vertical lines. By T_{μ_M,ν_A}^{max} we denote the maximum value of the quantity T_{μ_M,ν_A} considered as a function of γ_M.

From Fig. 2 we can see that during the ion escaping the surface, γ_{max} shifts from the value γ_ϕ toward the energy parameter γ_U. For a given R, the values γ_{max} can be compared with $\gamma_A(R)=[\tilde{\gamma}_A^2-(2Z-1)/(2R)]^{1/2}$. For $R=R_{in}^*$ we have $\gamma_{max}=\gamma_\phi=\gamma_A(R_{in}^*)$. At ion-surface distances $R=R_{in}^*+\Delta R$ for $n_A=6$ we have $\gamma_{max}=1.151$ and $\gamma_A(R)=1.150$, for $n_A=8$, we have $\gamma_{max}=0.794$ a.u. and $\gamma_A(R)=0.795$, and for $n_A=10$, we have $\gamma_{max}=0.676$ and $\gamma_A(R)=0.678$; all values (expressed in a.u.) are for $l_A=0$ and $m_A=0$. Finally, for $t \rightarrow t_{fin}$, we have $\gamma_{max} \approx \tilde{\gamma}_A=\gamma_A(R_{fin})$. For example, for $n_A=8, l_A=0, m_A=0$ we have $\gamma_{max}=1.067$ a.u. and
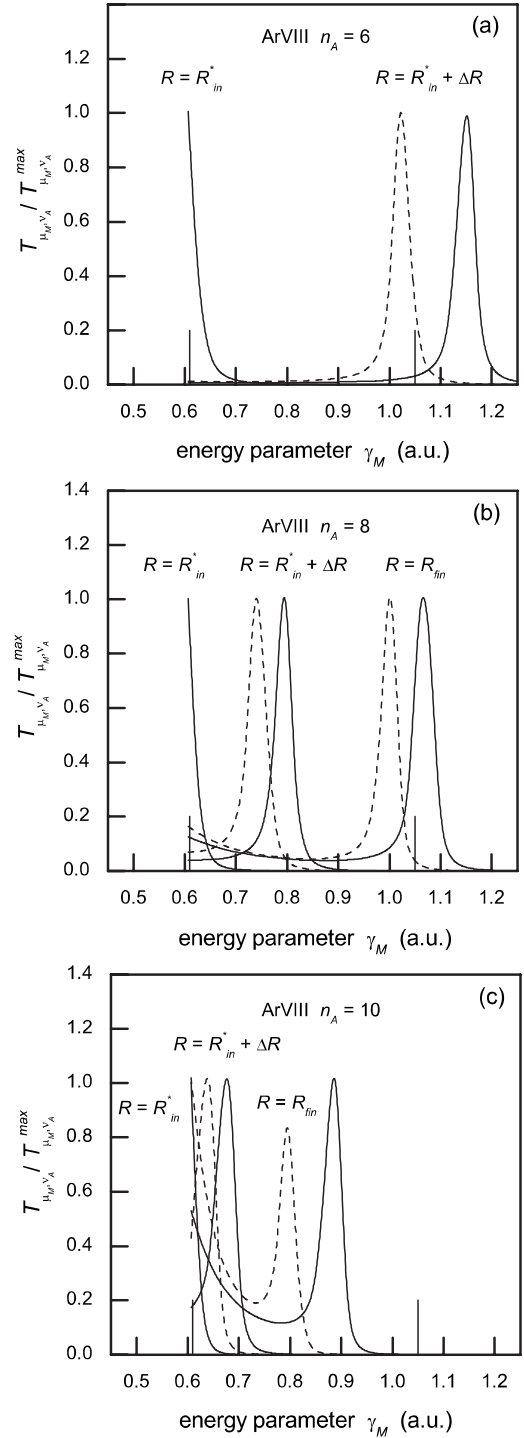

FIG. 2. Quantity $T_{\mu_M,\nu_A}/T_{\mu_M,\nu_A}^{max}$ for the population of Rydberg states $\nu_A=(n_A,l_A=0,m_A=0)$ for the Ar VIII ion ($v=0.01$ a.u.) with $n_A=$ (a) 6, (b) 8, and (c) 10, at ion-surface distances $R=R_{in}^*$, $R=R_{in}^*+\Delta R$ for $\Delta R=5$ a.u., and $R=R_{fin} \rightarrow \infty$. Dashed curves correspond to the pointlike ionic core case.

$\tilde{\gamma}_A=1.069$ a.u. Similar conclusions hold for $l_A \neq 0$ and for other sufficiently small ionic velocities v, as well as for the ions Kr VIII and Xe VIII.

From the above analysis, we conclude that

$$\gamma_{max} \approx \gamma_A(R). \qquad (4.2)$$

In fact, the quasiresonant condition (4.2) is well satisfied for the most relevant ion-surface distances ($R \approx R_c^N$). The discrepancy recognized in Fig. 2(c) for $R = R_{fin}$ is unimportant. Note that, for large R, we have $\gamma_{max} = \widetilde{\gamma}_A + O(1/R)$, in agreement with the assumption $\gamma_{max} \approx$ const used in the calculation of the normalized rate. The values γ_{max} given by Eq. (4.2) are independent of the projectile velocity v. In determination of γ_{max} we restricted the analysis to the values of γ_M corresponding to the initially occupied conduction band states (see the comment at the end of Sec. III A); hence, the quasiresonant condition, expressed by Eq. (4.2), is valid with accuracy $O(1/R^2)$. We point out that in the intermediate-velocity case ($v \approx 1$), the electron transitions are nonresonant [21–23].

Taking into account Eq. (4.2), as well as the fact that the position of the Firsov plane is determined by the parameter $g = 1/2$, we obtain $w = 0$ at all relevant ion-surface distances R. With this value of w, the expressions for the probability $\widetilde{P}_{\nu_A}(R)$ and the corresponding rate $\widetilde{\Gamma}_{\nu_A}(R)$, Eqs. (3.30) and (3.35), respectively, are significantly simplified. We get

$$\widetilde{P}_{\nu_A}(t) = \left[1 - \left(\frac{R}{R_{in}^*} \right)^{\widetilde{\alpha}} e^{-\widetilde{\beta}(R-R_{in}^*)} \right]^2, \qquad (4.3a)$$

$$\widetilde{\Gamma}_{\nu_A}(t) = 2v \left(\frac{R}{R_{in}^*} \right)^{\widetilde{\alpha}} \left(\frac{\widetilde{\alpha}}{R} - \widetilde{\beta} \right) e^{-\widetilde{\beta}(R-R_{in}^*)}$$
$$\times \left[\left(\frac{R}{R_{in}^*} \right)^{\widetilde{\alpha}} e^{-\widetilde{\beta}(R-R_{in}^*)} - 1 \right], \qquad (4.3b)$$

where $\gamma_M = \gamma_A(R)$. In the above equations we have $\widetilde{\beta} = (\gamma_M + \widetilde{\gamma}_A)/2$ and $\widetilde{\alpha} = Z/\widetilde{\gamma}_A - 1/2 + 1/(4\gamma_M)$, while R_{in}^* is given by Eq. (3.22).

Note that the probability $\widetilde{P}_{\nu_A}(t)$ is independent of the ionic velocity v; consequently, $\widetilde{\Gamma}_{\nu_A}(t) \sim v$, i.e., the quantity $\widetilde{\Gamma}_{\nu_A}(t)/v$ is also independent of v. Therefore, the image acceleration toward the surface that is present in the vicinity of the polarized solid has no influence on the intermediate quantities discussed within the framework of the time-symmetrized neutralization.

B. Intermediate stages of the Rydberg-level population for the ions Ar VIII, Kr VIII, and Xe VIII

The intermediate stages of the Rydberg-level population are characterized by the probability $\widetilde{P}_{\nu_A}(t)$ and rate $\widetilde{\Gamma}_{\nu_A}(t)$. In the absence of core polarization, the probabilities and rates for the ions Ar VIII, Kr VIII, and Xe VIII are the same. However, if the core polarization is taken into account, the values $\widetilde{\gamma}_A$, for the same values of n_A and l_A, become different for different ions (see Table I), so that the probabilities $\widetilde{P}_{\nu_A}(t)$ and rates $\widetilde{\Gamma}_{\nu_A}(t)$ will be modified, as well as the corresponding neutralization distances.

In Fig. 3 we present the probabilities $\widetilde{P}_{\nu_A}(t)$ and rates $\widetilde{\Gamma}_{\nu_A}(t)/v$ for $n_A = 6, 7, 8, 9$, and 10 and $l_A = 0$, $m_A = 0$, for the
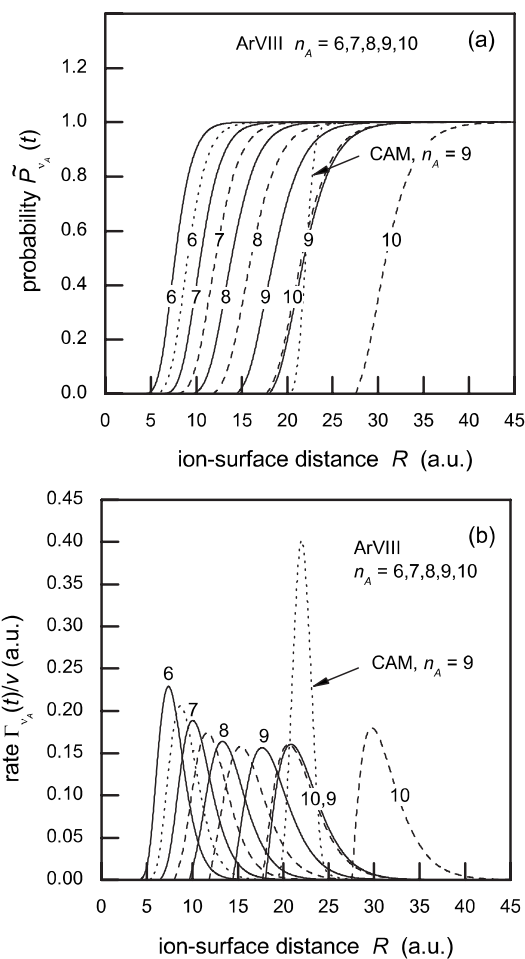

FIG. 3. (a) Probabilities $\widetilde{P}_{\nu_A}(t)$ and (b) rates $\widetilde{\Gamma}_{\nu_A}(t)/v$ for the population of the Rydberg state $\nu_A = (n_A, l_A = 0, m_A = 0)$ of the Ar VIII ion escaping the Al solid surface. Dashed curves correspond to the pointlike core case. The CAM curves in (a), (b) are the quantities $\widetilde{P}_{\mu_A}^{CAM}$ and $\widetilde{\Gamma}_{\mu_A}^{CAM}/v$ according to Ref. [7], respectively, for the neutralization of the O^{8+} ion with velocity $v = 0.01$ a.u., and for the Rydberg state $n_A = 9, n_{1A} = 0$, $m_A = 0$.

Ar VIII ion ($Z = 8$) slowly escaping the Al surface. The value $l_A = 0$ is chosen to emphasize the role of the core polarization. We point out that the final probability $P_{\nu_A}^{fin}$ increases with increasing l_A for $l_A = 0, 1$ and 2 [21]. The solid curves in Fig. 3 correspond to the polarized ionic cores; the dashed curves correspond to the pointlike cores ($\widetilde{\gamma}_A \rightarrow \gamma_{A0} = Z/n_A$). The same quantities, but for the ions Kr VIII and Xe VIII ($n_A \in [6,9], l_A = 0, m_A = 0$) are presented in Figs. 4 and 5, respectively.

From Figs. 3–5 we recognize the shift of the probabilities $\widetilde{P}_{\nu_A}(t)$ and rates $\widetilde{\Gamma}_{\nu_A}(t)$ toward larger ion-surface distances R with increasing n_A; at the same time, the polarization of the ionic core shifts the rates toward smaller ion-surface distances (compare the dashed curves with the full curves). The obtained shift of the rates $\widetilde{\Gamma}_{\nu_A}(t)$ induced by the polarization effect is characteristic for ions with the energy parameters $\widetilde{\gamma}_A > \gamma_{A0}$ (see Table I). The widths δ_{ν_A} of the presented rates increase with increasing n_A, which means that the neutralization process becomes more delocalized.
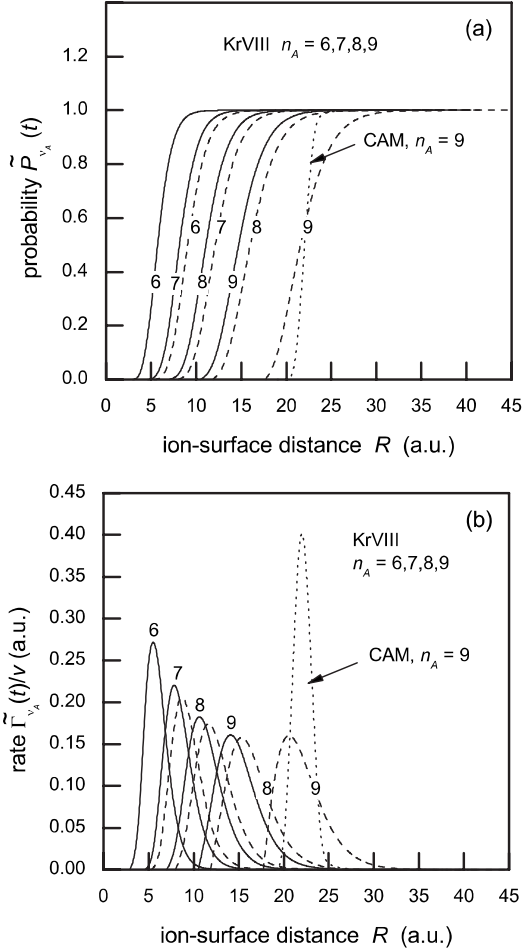
FIG. 4. (a) Probabilities $\widetilde{P}_{\nu_A}(t)$ and (b) rates $\widetilde{\Gamma}_{\nu_A}(t)/v$ for the population of the Rydberg state $\nu_A = (n_A, l_A=0, m_A=0)$ of the Kr VIII ion escaping the Al solid surface. Dashed curves correspond to the pointlike core case. The CAM curves in (a), (b) are the quantities $\widetilde{P}^{CAM}_{\mu_A}$ and $\widetilde{\Gamma}^{CAM}_{\mu_A}/v$ according to Ref. [7], respectively, for the neutralization of the O^{8+} ion with velocity $v=0.01$ a.u., and for the Rydberg state $n_A=9$, $n_{1A}=0$, $m_A=0$.
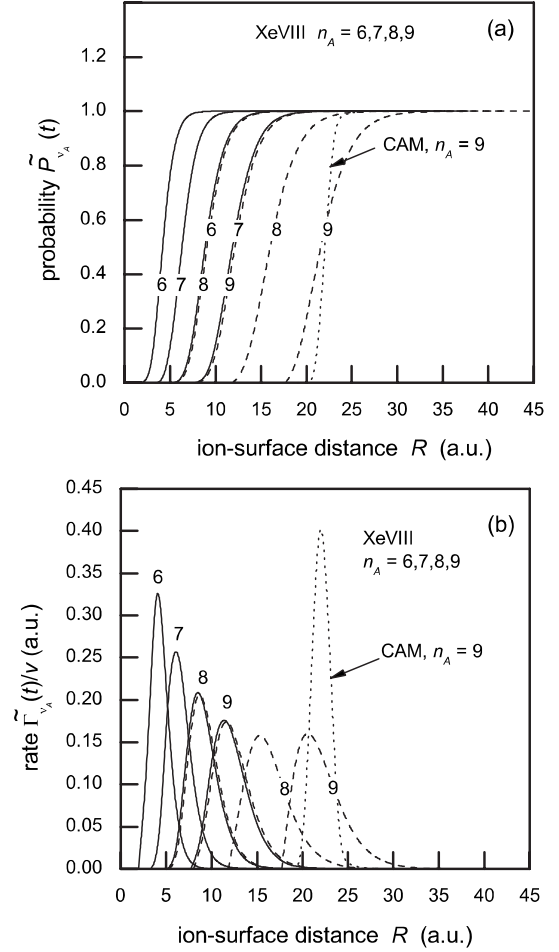
FIG. 5. (a) Probabilities $\widetilde{P}_{\nu_A}(t)$ and (b) rates $\widetilde{\Gamma}_{\nu_A}(t)/v$ for the population of the Rydberg state $\nu_A = (n_A, l_A=0, m_A=0)$ of the Xe VIII ion escaping the Al solid surface. Dashed curves correspond to the point like core case. The CAM curves in (a), (b) are the quantities $\widetilde{P}^{CAM}_{\mu_A}$ and $\widetilde{\Gamma}^{CAM}_{\mu_A}/v$ according to Ref. [7], respectively, for the neutralization of the O^{8+} ion with velocity $v=0.01$ a.u., and for the Rydberg state $n_A=9$, $n_{1A}=0$, $m_A=0$.

The rates presented in Figs. 3–5 can be compared with the available CAM theoretical results [7] only indirectly. That is, the hybridized states of the CAM method and the corresponding probabilities $P^{CAM}_{\mu_A}(t)$ and rates $\Gamma^{CAM}_{\mu_A}(t)$ are labeled (approximately) by the parabolic quantum numbers $\mu_A = (n_{2A}, n_{1A}, m_A)$; on the other hand, the states Ψ_1 and Ψ_2 correspond to the quantum numbers μ_M and ν_A, respectively, while the normalized neutralization rate $\widetilde{\Gamma}_{\nu_A}(t)$ is labeled by the spherical quantum numbers $\nu_A = (n_A, l_A, m_A)$. The low-l_A predictions of the present paper could be compared with the low-n_{1A} normalized CAM probabilities and rates defined in terms of semiclassical rate equation. That is, one can define the probability $P^{CAM}_{\mu_A}(t) = 1 - \exp(-\int_{t^*_{in}}^{t} \Gamma^{CAM}_{\mu_A}(t) dt)$, the normalized probability $\widetilde{P}^{CAM}_{\mu_A}(t) = P^{CAM}_{\mu_A}(t) / P^{CAM}_{\mu_A}(\infty)$, and the corresponding normalized rate $\widetilde{\Gamma}^{CAM}_{\mu_A}(t) = dP^{CAM}_{\mu_A}(t)/dt$. In Figs. 3–5 we present the quantities $\widetilde{P}^{CAM}_{\mu_A}(t)$ and $\widetilde{\Gamma}^{CAM}_{\mu_A}(t)/v$, calculated with the rates $\Gamma^{CAM}_{\mu_A}(t)$ taken from Ref. [7], in which the

neutralization of the fully stripped ion O^{8+} (i.e., the ionization of the O^{7+} ion) has been analyzed for the case $n_A=9$ and different values of n_{1A} and m_A. As states with large eccentricities, we consider states with $n_{1A}=0$, and for the ionic velocity we take the value $v=0.01$ a.u.; the value $R^*_{in} = 21$ a.u. is taken as the lower one for which the corresponding CAM rate is calculated in Ref. [7]. The normalized CAM probability and the corresponding rate indicate that the neutralization is almost instantaneously, localized at nearly the same position as it is predicted within the framework of the TVM, for the point-like core cases (dashed curves in Figs. 3–5).

In Fig. 6 we present the rates $\widetilde{\Gamma}_{\nu_A}(t)$ (scaled by v) for electron capture into the Rydberg states $\nu_A = (n_A=8, 10; l_A=0, 1, 2, 3; m_A=0)$ of the Ar VIII ion slowly escaping the Al surface. In the absence of core polarization (dashed curves in Fig. 6), the rates are independent of l_A; see Eq. (4.3b). If the core polarization is included, the rates shift toward smaller ion-surface distances R. This shift is significant for $l_A=0$, and becomes negligible for $l_A=3$.
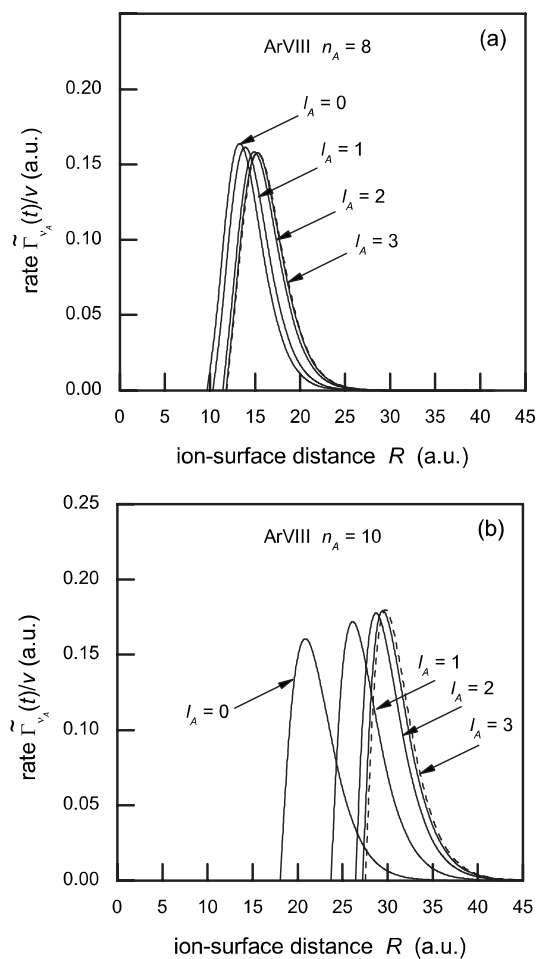
FIG. 6. Rates $\widetilde{\Gamma}_{\nu_A}(R)/v$ for the Ar VIII ion in the Rydberg states (a) $n_A=8$, $l_A=0,1,2,3$, and $m_A=0$, and (b) $n_A=10$, $l_A=0,1,2,3$, and $m_A=0$. Dashed curves correspond to the pointlike core case.

The maxima of the rates, exposed in Figs. 3(b), 4(b), 5(b), and 6, determine the neutralization distances R_c^N. In Table II we present the quantities R_c^N for the ions Ar VIII, Kr VIII, and Xe VIII. The presented neutralization distances R_c^N are independent of v.

The neutralization distances increase with increasing n_A, i.e., $R_c^N \sim Z/\widetilde{\gamma}_A \sim n_A^2/Z$, and, for a given n_A, the R_c^N values increase with increasing l_A, approaching the values obtained in absence of the core polarization (data in parentheses in Table II). The latter behavior is a consequence of the decreasing of $\widetilde{\gamma}_A$ with increasing l_A (see Table I). For example, $R_c^N = (1.7 + 0.1 l_A) n_A^2/Z$ a.u. in the case of the Ar VIII ion.

In Table II we also present the critical values R_c at which the energy level $E_A(R)$ becomes resonant with the potential barrier top. According to Ref. [19], in the absence of the core polarization we have $R_c = 2.38 n_A^2/Z$. If the ionic polarization is included, the critical distances can be estimated as $R_c \approx 2.38 \widetilde{n}_A^2/Z$, where $\widetilde{n}_A = Z/\widetilde{\gamma}_A$.

We point out that population of the levels ($n_A=11$; $l_A=0$; $m_A=0$) and ($n_A=12$; $l_A=0,1$; $m_A=0$) for Ar VIII (and for the other considered ions) is impossible. The same results hold if the polarization is neglected; in that case we have $P_{\nu_A}^{fin} \approx 0$ for the population of these Rydberg states. In Ref. [22] it was

demonstrated that, even in the nonresonant neutralization in the intermediate-velocity region, we have the thresholds ($n_{thr}=12$ for $l_A=1,2$, $m_A=0$ and $n_{thr}=11$ for $l_A=0$, $m_A=0$) in the corresponding final population distributions.

In Figs. 7(a)–7(c) we present the neutralization distances R_c^N for the population of the Rydberg states $\nu_A = (n_A, l_A=0, m_A=0)$ for Ar VIII, Kr VIII, and Xe VIII ions, respectively. Comparing the neutralization distances for the given n_A, we conclude from Fig. 7 that $R_c^N(\text{Xe VIII}) < R_c^N(\text{Kr VIII}) < R_c^N(\text{Ar VIII})$, i.e., the R_c^N values for Ar VIII are the closest to those obtained for the pointlike core case (dashed curves). The same conclusion is valid for $l_A \neq 0$ for the low-l_A cases considered. The quantities R_c^N presented in Fig. 7 represent the most probable ion-surface distances for the neutralization process. The finite widths δ_{ν_A} of the rates $\widetilde{\Gamma}_{\nu_A}(t)$ cause the process to be localized within the interval $[R_c^N - \delta_{\nu_A}/2, R_c^N + \delta_{\nu_A}/2]$; in Fig. 7 this fact is illustrated by bar symbols. The relative position of this interval with respect to $[R_{in}^*, R_c]$, indicates the character of the electron transitions: for $R \in [R_c^N - \delta_{\nu_A}/2, R_c^N + \delta_{\nu_A}/2] \cap [R_{in}^*, R_c]$ the transitions are mainly over-barrier in character; for the Rydberg states with $R_c^N + \delta_{\nu_A}/2 > R_c$ the tunneling process becomes important.

C. Comparison with experiments

The normalized probabilities $\widetilde{P}_{\nu_A}(t)$ tend to 1 for $t \to \infty$, so that the quantity $\widetilde{P}_{\nu_A}^{fin}$ cannot be used for a direct comparison with the experiments in which the final probability distributions or similar quantities (charge state, total yield, neutral fraction) are measured. The theoretical predictions of the TVM concerning the final population probabilities in the beam-foil geometry and comparison with the corresponding experiments are given in Refs. [21–23]. The main purpose of the present paper is to elucidate the intermediate stages of the process, characterized by the neutralization distances R_c^N.

At present, the experimental evidence for the considered ions exists only for projectiles impinging on the surface under grazing geometry, and only for very particular Rydberg states. The corresponding neutralization distances can be deduced from the measured projectile kinetic energy gains ΔE [27,28].

Assuming that the energy gain is due to the image acceleration, and that the projectile is completely and instantaneously neutralized at $R=R_c^N$, the quantities ΔE and R_c^N can be connected by the relation $\Delta E = Z^2/(4R_c^N)$. The neutralization distance R_c^N, calculated from the experimentally obtained energy gain, corresponds to electron capture from the Fermi level into the atomic energy level resonant with the potential barrier top $U_{eff,\eta}$, i.e., the quantity $R_c^N = Z^2/(4\Delta E)$ corresponds to the critical value n_c of the quantum number n_A. We recall that the critical quantum number n_c is defined by the condition $R_c = R_F$, where the Fermi distance R_F is defined by the condition $E_A(R_F) = -\phi$ and the critical distance R_c corresponds to the case $E_A(R_c) = U_{eff,\eta}(R_c)$; for the work function $\phi=5$ eV we get $n_c=10$ (in Ref. [19] the value $n_c=9$ corresponds to $\phi=4.2$ eV).

TABLE II. The neutralization distances R_c^N for the ions Ar VIII, Kr VIII, and Xe VIII obtained within the framework of the TVM and the critical distances R_c in (a.u.). Numbers in parentheses the are the neutralization distances and critical distances for point-like ionic cores.

n_A	$l_A = 0$	$l_A = 1$	$l_A = 2$	$l_A = 3$	R_c
Ar VIII					
6	7.4 (8.6)	7.8 (8.6)	8.4 (8.6)	8.7 (8.6)	(10.7)
7	10.0 (11.7)	10.6 (11.7)	11.3 (11.7)	11.6 (11.7)	(14.6)
8	13.3 (15.4)	13.9 (15.4)	15.0 (15.4)	15.3 (15.4)	(19.0)
9	17.7 (20.6)	18.4 (20.6)	20.1 (20.6)	20.6 (20.6)	(24.1)
10	20.8 (29.8)	26.2 (29.8)	28.7 (29.8)	29.4 (29.8)	(29.7)
11	(48.3)	40.4 (48.3)	45.3 (48.3)	49.3 (48.3)	(36.0)
12	(99.2)	(99.2)	91.0 (99.2)	98.7 (99.2)	(42.8)
Kr VIII					
6	5.5 (8.6)	6.0 (8.6)	7.1 (8.6)	8.5 (8.6)	(10.7)
7	7.8 (11.7)	8.4 (11.7)	9.7 (11.7)	11.3 (11.7)	(14.6)
8	10.6 (15.4)	11.4 (15.4)	12.8 (15.4)	15.0 (15.4)	(19.0)
9	14.1 (20.6)	15.0 (20.6)	16.9 (20.6)	19.9 (20.6)	(24.1)
Xe VIII					
6	4.1 (8.6)	4.4 (8.6)	5.4 (8.6)	7.2 (8.6)	(10.7)
7	6.1 (11.7)	6.6 (11.7)	7.8 (11.7)	9.9 (11.7)	(14.6)
8	8.7 (15.4)	9.2 (15.4)	10.6 (15.4)	13.1 (15.4)	(19.0)
9	11.4 (20.6)	12.2 (20.6)	13.9 (20.6)	17.2 (20.6)	(24.1)

In the escaping geometry considered in the present paper, the empty level $n_A = 10$ is the highest one that can be resonantly populated (from the Fermi level), so that the neutralization distances for $n = n_c$ (and independently of l_A) can be estimated from the values obtained on the basis of energy gains; for the simulation of energy gain within the framework of the COB model, see Ref. [4]. The corresponding values are presented in Figs. 7(a) and 7(c) for the ions Ar VIII and Xe VIII, respectively (full dots); in both cases we use the scaling $\Delta E \sim Z^{3/2}$ [4] to obtain the energy gains for the case of $Z = 8$ from the available experimental data [27,28]. We point out that the first neutralization distance proposed by the COB method is given by $R_c^N = \sqrt{8Z+2}/(2\phi)$ [3,37]. For the case considered in the present paper the last formula yields $R_c^N = 22.09$ a.u., the empty dots in Fig. 7.

From Fig. 7(a), in which we analyze the localization of the charge exchange into the Rydberg levels of Ar VIII, we conclude that the TVM R_c^N value for $n = n_c$ lies between the value derived from the experimentally obtained energy gain [27] (full dot) and the value estimated by the COB expression [3,37] (empty dot). In the case of the Xe VIII ion, Fig. 7(c), and for $n_A = n_c$, only the values for the neutralization distances in the absence of core polarization are available (dashed curves), so that the comparison with experiment [28] yields only a qualitative agreement.

We point out that the experimental setup [27,28] used in the measurement of the energy gain and the TVM theoretical considerations of the present paper are devoted to different physical problems, cascade neutralization in grazing impact geometry and neutralization in the escaping geometry with the postselected final state $\nu_A = (n_A, l_A, m_A)$.

D. Complementarity of the neutralization and ionization processes

The neutralization and ionization processes at solid surfaces of multiply charged ions (escaping and approaching surfaces, respectively; see Fig. 8) can be considered as two complementary processes.

In Fig. 9 we present the neutralization probabilities $\tilde{P}_{\nu_A}(t)$ and rates $\tilde{\Gamma}_{\nu_A}(t)$ obtained in the present paper and EEM ionization probabilities $P_{\mu_A}^I(t)$ and the corresponding total rates $\tilde{\Gamma}_{\mu_A}^I(t)$ taken from Ref. [19]; by ν_A and μ_A we denote the atomic spherical and atomic parabolic quantum numbers, respectively. The neutralization probabilities [solid curves in Fig. 9(a)] increase from zero to unity, when the ions escape the surface, while the ionization probabilities [dashed curves in Fig. 9(a)] have the same behavior when the ions approach the surface. From Fig. 9(b) we conclude that the rates $\tilde{\Gamma}_{\nu_A}(t)$ and $\tilde{\Gamma}_{\mu_A}^I(t)$ offer complementary evidence about the electron exchange process.

The discussed neutralization and ionization processes are mainly localized at distances R_c^N and R_c^I (positions of the maxima of the corresponding rates). In Table III we present the R_c^N and R_c^I values for the pointlike core charge $Z = 8$. In Table III we also present the corresponding Fermi distances R_F: $E_A(R_F) = -\phi$. Note that the Fermi distance represents the initial ion-surface distance for the neutralization $[R_F = R_{in}^*$; see Eq. (3.22)]. If neutralization and ionization are possible for the same n_A (in the case $n_A = n_c = 10$, for $\phi = 5$ eV), we have $R_c^I \approx R_c^N$. For $n_A \neq n_c$, the values R_c^I are complementary to the R_c^N values.
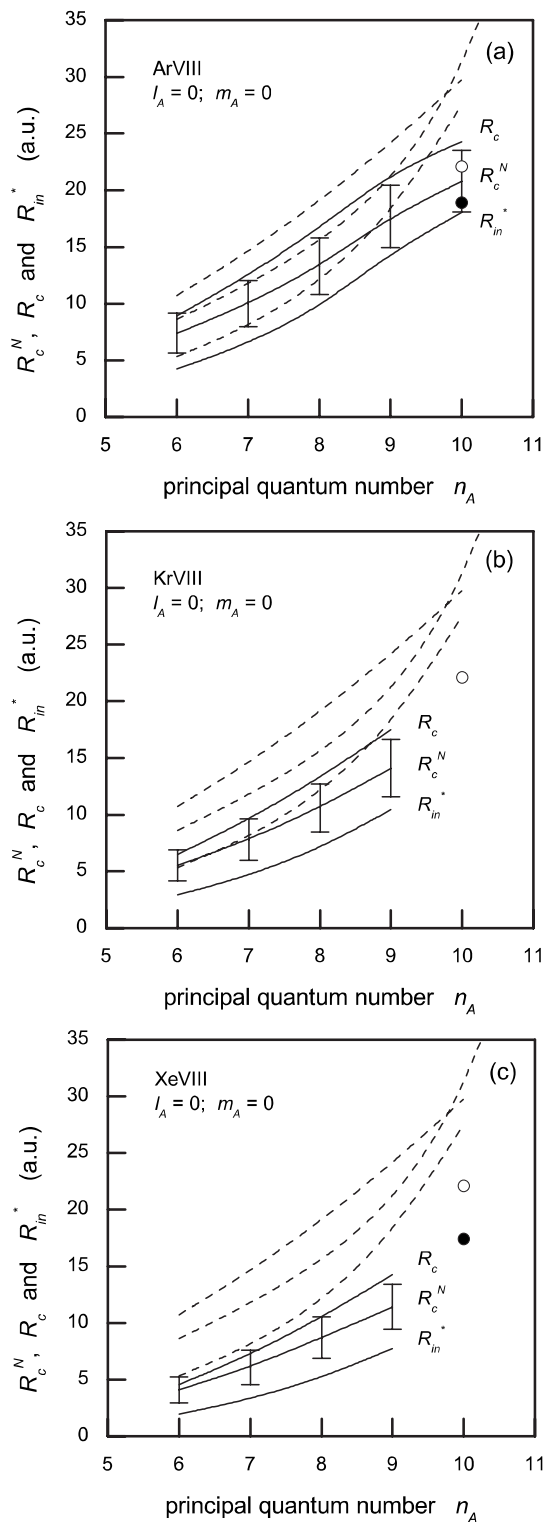
FIG. 7. Neutralization distances R_c^N, critical distances R_c, and initial distances R_{in}^* (solid curves) for the Ar VIII, Kr VIII, and Xe VIII ions ($Z=8$), escaping the Al surface with $v \ll 1$ a.u., for electron capture into the Rydberg state $\nu_A=(n_A, l_A=0, m_A=0)$. Dashed curves correspond to the pointlike core case. The bar symbols are the values δ_{ν_A} (a.u.). By the full dots in (a) and (c) we mark the neutralization distances derived from the measured energy gains, [27] and [28], respectively. Empty dots are the COB values [3,37].
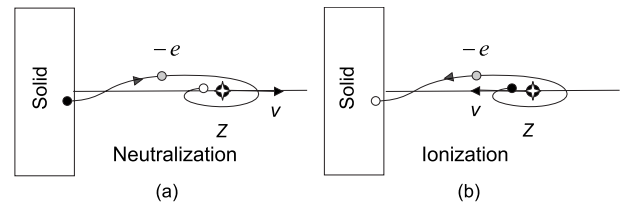

FIG. 8. Schematic of neutralization of A^{Z+} ion and ionization of $A^{(Z-1)+}$ ion moving in two opposite directions with respect to the surface.

In Fig. 10 we present the neutralization distances R_c^N and ionization distances R_c^I, as well as the distances R_F and the critical distances R_c, for the two processes considered and for the pointlike core charge $Z=8$. The value $n_c=10$ is marked by an arrow. The R_c^N and R_c^I curves increase with increasing n_A and intersect in the vicinity of $n_A=n_c$. In the same figure, we present (bar symbols) the widths δ_{ν_A} and $\delta_{\mu_A}^I$ of the rates
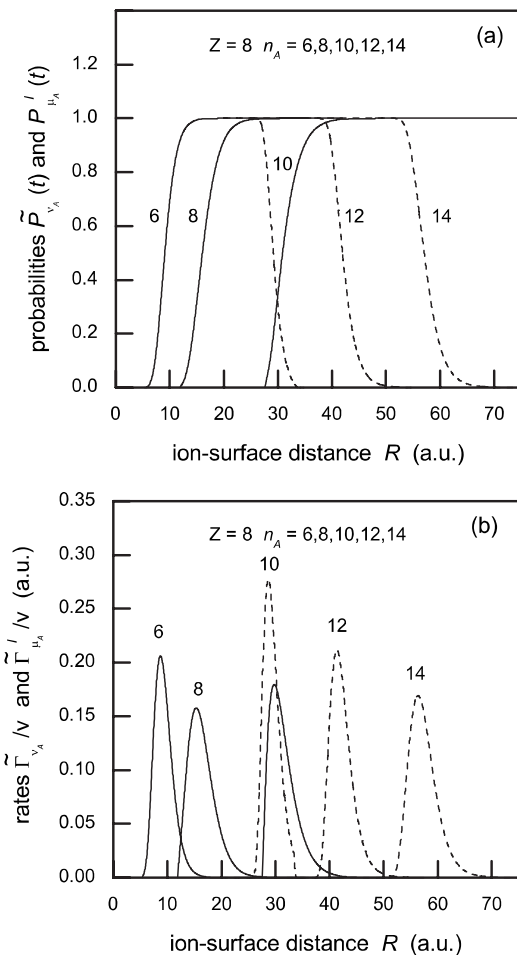

FIG. 9. Neutralization (solid curves) of A^{8+} ion escaping the Al surface with velocity $v \ll 1$ a.u., for the population of the Rydberg state $\nu_A=(n_A, l_A=0, m_A=0)$, and ionization [19] (dashed curves) of A^{7+} ion in the Rydberg state $\mu_A=(n_A, n_{1A}=0, m_A=0)$ approaching the Al surface with velocity $v=0.01$ a.u. (a) The neutralization probabilities $\widetilde{P}_{\nu_A}(t)$ and the ionization probabilities $P_{\mu_A}^I(t)$, and (b) the rates $\widetilde{\Gamma}_{\nu_A}(t)$ and $\widetilde{\Gamma}_{\mu_A}^I(t)$ scaled by v (in atomic units). All curves are for the pointlike core charge $Z=8$.

TABLE III. Neutralization distances R_c^N for $\nu_A=(n_A,l_A=0,m_A=0)$ and ionization distances R_c^I [19] for $\mu_A=(n_A,n_{1A}=0,m_A=0)$ and $v=0.01$ a.u. and Fermi distances R_F, for pointlike core charges $Z=8$ and Al surface.

	n_A				
	6	8	10	12	14
R_c^N (a.u.)	8.6	15.4	29.8	99.2	
R_c^I (a.u.)			28.7	41.3	56.6
R_F (a.u.)	5.3	11.9	27.5	97.7	

$\widetilde{\Gamma}_{\nu_A}(t)$ and $\widetilde{\Gamma}_{\mu_A}^I(t)$, respectively. Considering the intervals of the neutralization (ionization) localization, we conclude that the processes are mainly overbarrier. The exceptions are the lower n_A values in the case of neutralization and the higher n_A values in the case of ionization, in which the subbarrier transitions become significant.

The relation $\widetilde{\Gamma}_{\nu_A}(t)\approx\widetilde{\Gamma}_{\mu_A}^I(t)$ that holds in the special case $n_A=n_c$, and the agreement of the $\Gamma_{\mu_A}^I(t)$ with the CAM neutralization rate $\Gamma_{\mu_A}^{CAM}(t)$ [6,7] for the critical quantum number n_c (see Fig. 2 in Ref. [19]), confirm the statement that the TVM presented in this paper and the CAM method are comparable for the discussed combination of quantum numbers ν_A and μ_A. We point out that the time-symmetrized TVM and the CAM method are related to different formulations of the problem.

V. CONCLUDING REMARKS

In this paper we presented a time-symmetrized neutralization model (two-state vector model), adapted for the low-velocity case. The Rydberg-level population of multiply
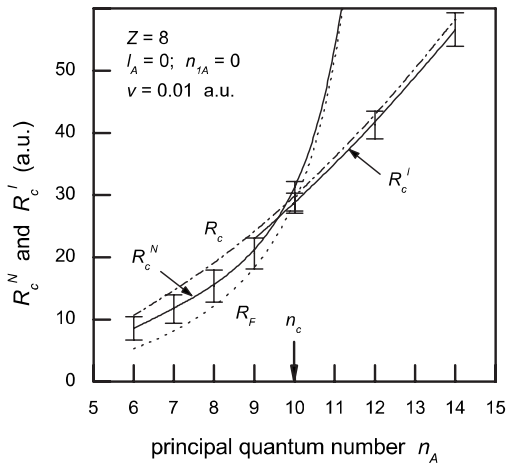

FIG. 10. Neutralization distances R_c^N for the ion $Z=8$ escaping the Al surface with $v\ll1$ a.u., with electron capture into the Rydberg state $\nu_A=(n_A,l_A=0,m_A=0)$, and ionization distances R_c^I of the ion $Z=8$ in the Rydberg state $\mu_A=(n_A,n_{1A}=0,m_A=0)$ approaching the Al surface with $v=0.01$ a.u. [19]. Dotted and dot-dashed curves are the Fermi distances R_F and critical distances R_c, respectively. The bar symbols are the values δ_{ν_A} and $\delta_{\mu_A}^I$ in a.u.

charged ions (Ar VIII, Kr VIII, and Xe VIII) escaping a solid surface was considered, for electron capture into the state $\nu_A=(n_A,l_A,m_A)$. Both the solid polarization and the ionic core polarization effects are taken into account. The normalized neutralization probability $\widetilde{P}_{\nu_A}(t)$ and the corresponding rate $\widetilde{\Gamma}_{\nu_A}(t)$ are obtained in a very simple analytical form, Eqs. (4.3a) and (4.3b). The quantities $\widetilde{P}_{\nu_A}(t)$ and $\widetilde{\Gamma}_{\nu_A}(t)$, describe the intermediate stages of the neutralization, under the fixed final-state condition $|\Psi_2(t_{fin})\rangle=|\nu_A\rangle$ and for all possible initial states $|\Psi_1(t_{in})\rangle=|\mu_M\rangle$ where $\mu_M=(\gamma_M,n_{1M},m_M)$.

The characteristic feature of the TVM in the low-velocity regime is the quasiresonant character of the electron transitions. That is, the probability density distribution $T_{\mu_M,\nu_A}(t)$ [Eq. (4.1)] over the energy parameter γ_M of the active electron is well localized (at $\gamma_M=\gamma_{max}$), and shifts during the ionic motion, synchronized with the shift of the energy $E_A(R)$ of the ionic Rydberg state, i.e., $\gamma_{max}=\gamma_A(R)$. From the rates $\widetilde{\Gamma}_{\nu_A}(t)$, the neutralization distances R_c^N are obtained, for electron capture into high-eccentricity Rydberg states $n_A \in[6,12]$, $l_A\in[0,3]$, and $m_A=0$. The obtained values of R_c^N along with the widths δ_{ν_A} of the rates $\widetilde{\Gamma}_{\nu_A}(t)$ enabled us to identify the localization and the overbarrier-subbarrier character of the neutralization process.

We also demonstrated that the time-symmetrized neutralization of the ion A^{Z+} escaping the surface and the EEM ionization of the ion $A^{(Z-1)+}$ approaching the surface [19] are complementary. In the special case $n_A=n_c$, we have $\widetilde{\Gamma}_{\nu_A}\approx\widetilde{\Gamma}_{\mu_A}^I$. From the analysis of the $n_A=n_c$ case, it was also concluded that the normalized neutralization probabilities $\widetilde{P}_{\nu_A}(t)$ and rates $\widetilde{\Gamma}_{\nu_A}(t)$ obtained in the present paper are in agreement with the corresponding quantities of CAM method [6,7], at least for some combinations of quantum numbers ν_A and μ_A. That is, the neutralization distances predicted by the TVM and CAM method are nearly the same, but the TVM predicts more delocalized neutralization (the widths δ_{ν_A} of the TVM rates are twice the CAM rate widths). By using the experimental data for the projectile energy gain [27,28], obtained for the ions impinging the surface in the grazing geometry, we deduced the neutralization distances for $n=n_c$; the values so obtained are also in agreement with the R_c^N values calculated in the present paper. However, the cited experimental data are not conclusive enough for the quantum predictions of the time-symmetrized TVM approach.

Few additional comments may be relevant for further investigations of the time-symmetrized neutralization of the multiply charged ions interacting with solid surfaces.

First, the TVM treatment of the intermediate stages of the neutralization in the present paper is devoted to the small ionic velocities ($v\ll1$) and the low-l_A Rydberg states. This treatment can be extended to the intermediate velocity case ($v\approx1$); the key difference in respect to the low-velocity case, is that the electron transitions become nonresonant [21,22]. Our preliminary calculations of the corresponding probabilities and rates for the S VI, Cl VII, and Ar VIII ions escaping the surface with intermediate velocities, indicate

that two different R regions can be distinguished. Closer to the surface, the neutralization is unstable; the probabilities and rates are oscillatory in character. At larger ion-surface distances R the neutralization is stabilized; the behavior of the probabilities and rates becomes similar to that obtained in the present paper.

Second, the extension of the TVM developed in the present paper to the large-l_A Rydberg states of multiply charged ions is possible, taking into account that the corresponding electron transitions do not take place in the vicinity of the z axis. The final population probability treatment within the framework of the TVM in the intermediate velocity region, that takes into account a wide space region around the projectile trajectory, was developed in Ref. [23]. The treatment of the intermediate stages of the population will be worthwhile. We point out that the recent experimental data for the final population probabilities of the multiply charged Rydberg ions Ar^{7+} and Ar^{8+} are obtained for the large-l_A case and ionic velocities $v \approx 0.2$ a.u., implying the microcapillary foil [38]; the population of the levels $n_A = 7, 8, \ldots, 11$ ($n_A \leq n_c$ and $n_A > n_c$) was reported. The experimentally obtained probability distributions could be obtained from the large-l_A TVM of the nonresonant neutralization accompanied by the reionization.

Finally, the full two-state description (with fixed initial and final states) of the intermediate stages of the Rydberg-level population could be possible on the bases of Eq. (3.32) for $T_{\mu_M, \nu_A}(t)$. It is indicative that the probability $T_{\mu_M, \nu_A}(t)$ per unit γ_M, considered as a function of the ion-surface distances R, has the maximum at $R = \mathcal{R}_c^N(\mu_M, \nu_A)$, which satisfies the quasiresonant condition $\gamma_M = \gamma_A(\mathcal{R}_c^N)$. This fact can be used to elucidate the role of the surface states of the solid in the neutralization process.

ACKNOWLEDGMENTS

[1] J. Burgdörfer, in *Review of Fundamental Processes and Applications of Atoms and Molecules*, edited by C. D. Lin (World Scientific, Singapore, 1993).

[2] J. Burgdörfer, P. Lerner, and F. W. Meyer, Phys. Rev. A **44**, 5674 (1991).

[3] J. J. Ducrée, F. Casali, and U. Thumm, Phys. Rev. A **57**, 338 (1998).

[4] J. J. Ducrée, H. J. Andrä, and U. Thumm, Phys. Rev. A **60**, 3029 (1999).

[5] U. Wille, Phys. Rev. B **50**, 1888 (1994).

[6] D. Teillet-Billy and J. Gauyacq, Surf. Sci. **239**, 343 (1990).

[7] A. G. Borisov, R. Zimny, D. Teillet-Billy, and J. P. Gauyacq, Phys. Rev. A **53**, 2457 (1996).

[8] P. Nordlander and J. C. Tully, Phys. Rev. Lett. **61**, 990 (1988).

[9] P. Nordlander and J. C. Tully, Phys. Rev. B **42**, 5564 (1990).

[10] P. Nordlander, Phys. Rev. B **53**, 4125 (1996).

[11] J. Hanssen, C. F. Martin, and P. Nordlander, Surf. Sci. **423**, L271 (1999).

[12] V. A. Mandelshtam, T. R. Ravuri, and H. S. Taylor, Phys. Rev. Lett. **70**, 1932 (1993).

[13] J. Müller, X. Yang, and J. Burgdörfer, Phys. Rev. A **49**, 2470 (1994).

[14] P. Kürpick and U. Thumm, Phys. Rev. A **54**, 1487 (1996).

[15] P. Kürpick, U. Thumm, and U. Wille, Phys. Rev. A **57**, 1920 (1998).

[16] J. Sjakste, A. G. Borisov, and J. P. Gauyacq, Phys. Rev. A **73**, 042903 (2006).

[17] Lj. D. Nedeljković and N. N. Nedeljković, Phys. Rev. A **67**, 032709 (2003).

[18] N. N. Nedeljković and Lj. D. Nedeljković, Phys. Rev. A **72**, 032901 (2005).

[19] Lj. D. Nedeljković, N. N. Nedeljković, and D. K. Božanić, Phys. Rev. A **74**, 032901 (2006).

[20] N. N. Nedeljković, Lj. D. Nedeljković, R. K. Janev, and Z. L. Mišković, Nucl. Instrum. Methods Phys. Res. B **58**, 519 (1991).

[21] N. N. Nedeljković, Lj. D. Nedeljković, S. B. Vojvodić, and M. A. Mirković, Phys. Rev. B **49**, 5621 (1994).

[22] Lj. D. Nedeljković and N. N. Nedeljković, Phys. Rev. B **58**, 16455 (1998).

[23] N. N. Nedeljković, Lj. D. Nedeljković, and M. A. Mirković, Phys. Rev. A **68**, 012721 (2003).

[24] S. B. Hill, C. B. Haich, Z. Zhou, P. Nordlander, and F. B. Dunning, Phys. Rev. Lett. **85**, 5444 (2000).

[25] S. Wethekam, H. R. Dunham, J. C. Lancaster, and F. B. Dunning, Phys. Rev. A **73**, 032903 (2006).

[26] G. R. Lloyd, S. R. Procter, and T. P. Softley, Phys. Rev. Lett. **95**, 133202 (2005).

[27] H. Winter, Europhys. Lett. **18**, 207 (1992).

[28] H. Winter, C. Auth, R. Schuch, and E. Beebe, Phys. Rev. Lett. **71**, 1939 (1993).

[29] Y. Aharonov, P. G. Bergmann, and J. L. Lebowitz, Phys. Rev. **134**, B1410 (1964).

[30] B. Reznik and Y. Aharonov, Phys. Rev. A **52**, 2538 (1995).

[31] Yu. N. Demkov and V. N. Ostrovskii, Zh. Eksp. Teor. Fiz. **69**, 1582 (1975).

[32] J. Barden, Phys. Rev. Lett. **6**, 57 (1961).

[33] G. Simons and A. N. Bloch, Phys. Rev. B **7**, 2754 (1973).

[34] N. Fröman and P. O. Fröman, *JWKB Approximation* (North-Holland, Amsterdam, 1965).

[35] N. N. Nedeljković, Fizika (Zagreb) **12**, 275 (1980).

[36] Yu. Ralchenko, F. C. Yoy, D. E. Kelleher, A. E. Kramida, A. Musgrove, J. Reader, W. L. Wiese, and K. Olsen, NIST Atomic Spectra Database, http://physics.nist.gov/PhysRefData/ASD/levels_form.html

[37] J. Burgdörfer and F. Meyer, Phys. Rev. A **47**, R20 (1993).

[38] Y. Morishita *et al.*, Phys. Rev. A **70**, 012902 (2004).